Università degli Studi di Napoli Federico II

Facoltà di Ingegneria
Dipartimento di Informatica e Sistemistica

Tesi di Dottorato di Ricerca in Ingegneria Informatica ed Automatica
Coordinatore: Prof. Francesco Garofalo
Novembre 2011

Grasping algorithms for anthropomorphic robotic hands inspired to human behavior

by

Francesca Cordella

Thesis Supervisor: **Prof. Bruno Siciliano**

Submitted to the Faculty of Engineering, University of Naples Federico II, in partial fulfillment of the requirements for the degree of Doctor of Philosophy.

Printed in Italy.
Napoli, November 2011.

To my Father, my Mother and my Sister

Acknowledgements

I sincerely thank Prof. Bruno Siciliano for giving me the opportunity to carry out my work in his research group and for his always valuable advices. His lectures on robotics prompted me to undertake my PhD in this field. Thanks are due to him also for introducing me to Dott. Loredana Zollo who deserves a special mention.

I am particularly grateful to Loredana for making possible my collaboration with her at Campus Biomedico in Rome. I hold her in great esteem: her competence and constant kind assistance have been essential during the development of my work. Her constructive advices have been fundamental for allowing me to improve my knowledge in the field of medical robotics.

I also thank Dott. Patrick van der Smagt for giving me the chance to work at DLR in Munich under his supervision. Among the members of DLR team I would also particularly thank Dott. Claudio Castellini, Georg Stillfried and Agneta Gustus.

I would like to thank also Prof. Stefano Ricciardi for allowing me to work with the CyberGlove in the Virtual Reality Lab of the University of Salerno.

Among the people I met during these three years I would like to thank Antonino Salerno, who worked with me for testing the algorithm on the robotic platform.

I cannot omit to mention all my friends: they were always near to me with their friendly and encouraging words.

Last, but not least, a big "thank you" goes to my "first reviewer", always present with a smile.

Prologue

Biologically inspired robotic systems are becoming increasingly popular, especially in the field of medical robotics, in which building robotic devices able to replicate the human behavior guarantees obtaining motor recovery, functional substitution or human-robot interaction as human-like as possible. It is widely recognized that robotic rehabilitation devices improve the performance of the rehabilitation therapy performed by a human therapist in terms of action repetition and accurate tracking of the desired trajectory. Taking advantage from the plasticity of the neuro-muscular system, a human-inspired robotic rehabilitation therapy helps patients to re-learn movements. In the field of upper limb prosthetics, since the aim of a prosthetic hand is to replace a human hand, the robotic device has to be not only functional, but also as similar as possible to the human one both from the morphological point of view and as regards movement naturalness. On the other hand, since grasping is one of the human skills that robotic researchers mostly attempt at imitating, in the development of new robotic hands, the inspiration to the human hand behavior is increasing.

From the analysis of the grasping action performed by human beings and from the study of the anatomy of the human hand and of its behavior during grasping, it is possible to obtain useful information for developing human-like grasping algorithms so as to acquire a better knowledge of the hand kinematics in order to design new human-like robotic hands and new rehabilitation devices. The definition of the kinematic structure of the hand and of the fingers is, in fact, the basis for designing new dexterous robotic hands and devices devoted to

interact with the human hand (such as rehabilitation devices). Therefore this work is focused on the study of the hand kinematics, providing the basis for a further study regarding the hand dynamics. All the experiments done are in fact adaptable for a future study of the hand dynamics.

In assistive robotics, as well as in the field of hand prostheses, the ability of performing smooth movements and obtaining a stable grasp is essential. Therefore, one of the aims of this thesis is to develop a bio-inspired approach for posture prediction and finger trajectory planning with a robotic hand. In order to do that, the human grasping action has been deeply analyzed. It has been decomposed in three main phases: reaching, pre-shaping and grasping. During reaching, the hand approaches the object to be grasped. The most appropriate finger configuration to ensure a stable grasp is defined during preshaping. Then, the full-blown grasp follows. In order to reduce the complexity of planning dexterous hand grasps, it is useful to find the best hand preshape: therefore, this work is focused on this grasping phase. An accurate analysis of anatomy, surgery and rehabilitation literature has been done. In order to confirm the literature results and to cope with the lack of information, e.g. about thumb behavior, different methods for acquiring information about the human hand behavior have been used. Some important features about grasping have been collected from the analysis of the data obtained from two different devices for movement analysis: the Vicon system and a sensorized glove (the CyberGlove). The hand joint behavior during the grasping action has been analyzed asking different subjects to realize four different grasping tasks. The selected tasks guarantee that the subjects pose the hand in the most commonly used configurations. The experiments were performed asking subjects to wear the CyberGlove or attaching on their hands markers visible by the Vicon cameras. The obtained data have been analyzed using different hand kinematic human-inspired models. In order to overcome the drawbacks of the motion analysis devices listed before (such as the not completely natural movements performed wearing a data glove, the impossibility to use the CyberGlove from people of different hand sizes and the high cost of the Vicon system), and to obtain

information about the hand movements, the Kinect® motion sensing device has also been used. For determining the finger joint positions and trajectories during hand movements, a finger tracking algorithm for the Kinect camera has been implemented. Blue markers have been placed on the hand joints following the same configuration used in the experiments performed with the Vicon cameras. A coloured blob detection algorithm and a multiple object tracking algorithm based on particle filters and extended Kalman filter has been implemented.

When observing the human grasping behavior, thanks to the input devices listed before, it has been possible to notice some common characteristics among different subjects. The literature results about the dependence of grasping shape on object properties and grip types have been confirmed. The relationship between hand joints for each subject and among different subject has been investigated. One of the obtained results has been finding a constant value of the hand aperture angle (the angle between thumb and index finger). Also the curvature of the fingers is constant among different subjects (related to hand dimensions). Therefore, on the basis of neurological studies and of the analysis of the obtained data, a bio-inspired algorithm for predicting the power-grip posture and planning the finger trajectory of a robotic hand has been developed. The method estimates the best joint hand configuration during diagonal and transverse volar grasp minimizing a purposely defined objective function given by the sum of the joint distances from the object center of rotation (COR). The developed grasping algorithm calculates the position of the fingers for grasping, finding the best hand configuration that ensures a stable human-like grasp. The implementation of the algorithm on a real robotic platform has validated its effectiveness.

From the above discussion, it is clear that the aim of this work is to find a way of exploiting the knowledge about a natural system, namely the human hand, in order to design a robotic system. After investigating and understanding in depth the human grasping action, the obtained results have multiple applications such as:

- overcoming the structural lack of the actual robotic hands (for instance, the

non opposable thumb);

- developing new interfaces for rehabilitation (the finger tracking algorithm developed for the Kinect motion sensing device could be a new rehabilitation interface with potential application in the rehabilitation field);
- developing bio-inspired approaches for posture prediction and finger trajectory planning in order to perform a stable human-like grasp with a robotic hand.

In detail, the structure of the thesis is the following:

- In Chapter 1, a brief introduction about bio-inspired robotic devices and the main motivations for studying and imitating the human behavior during grasping are provided. Further, a rough description of the grasping action and an explanation of the reasons for choosing to focus the work on the preshaping phase and on the kinematic aspect of grasping are given. Finally, the thesis topics are summarized.
- In Chapter 2, the state of the art of the studies on human hand is analyzed, paying particular attention to the hand anatomy and its kinematic structure. A comparison between the hand kinematics and the kinematic models of the actual robotic hands is performed.
- In Chapter 3, in order to validate the available results in the literature and to cope with the lack of information, e.g. about thumb behavior, the devices used for hand movement analysis are introduced. After a brief description of the devices, the protocol used for the experiment is illustrated, demonstrating the validity of each choice. The experiments realized with the CyberGlove and the Vicon system are described and the obtained results are analyzed.
- In Chapter 4, the Kinect camera is introduced in the attempt of overcoming the drawbacks of the devices described in Chatper 3 for the analysis of

hand motion. A marker tracking algorithm for estimating the hand joint positions is presented and discussed. A possible application in creating a new rehabilitation interface, utilizing a finger tracking algorithm that is also described, is introduced.

- In Chapter 5, the results obtained from the experiments described in Chapter 3 are used for implementing a bio-inspired power-grip posture prediction algorithm and a finger trajectory planning algorithm. Algorithm effectiveness has preliminarily been tested by means of simulation trials. Then, experimental trials on a real arm-hand robotic system have been carried out, in order to validate the approach and to evaluate algorithm performance.

- Chapter 6 is devoted to conclusions and future work.

Contents

List of Figures

List of Tables

Chapter 1

Introduction

A wide analysis of the field of robotics applied to rehabilitation, prosthetics and manipulation [1], [2] has shown an increasing interest for the realization of devices able to replicate the human behavior. The bio-inspiration enables:

- designing rehabilitation robotic devices assuring a therapy for motor recovery more similar to that effected by a human therapist;
- substituting the functionality of a missing limb with robotic prostheses exhibiting physical and functional features as much as possible similar to the human ones;
- realizing a human-robot interaction as safe and natural as possible;
- to realize robotic hands with special dexterity features.

The work illustrated in this thesis draws inspiration from studies made on human beings, with special reference to the analysis of the human hand behavior during the grasping operation. In order to apply the studies that will be described in the following to the fields listed above, a few hypotheses widely confirmed in the literature have been accepted.

Rehabilitation robotic devices [3], [4], [5], [6] aim to help the patient regain learning on how to move by exploiting the plasticity of the neuromuscular system,

that is its ability to learn again the motor patterns thanks to the repeated execution of pre-established movements. Medical studies [7], [8] have evidenced that, as a consequence of a neuromuscular damage, the human motor system has to learn again the right spatio-temporal scheme of muscle activation. With respect to the human therapist, the robot for rehabilitation guarantees greater accuracy as regards action iteration and follow-up of the desired trajectories [9]. Upper limb robotic prostheses should be as much as possible similar to human limbs (as for size, weight and shape) and at the same time they should guarantee dexterity, stability, grasping adaptability and movement naturalness [10], [11], [12], [13].

Since the human hand is an example of high dexterity system above all others, it is clear that, when developing robotic hands, the interest to replicate the human hand ability is increased. The analysis of the problems encountered in the realization of robotic devices able to faithfully reproduce the operations performed by humans, such as just grasping, has led us to thoroughly study the bio-inspired grasping problem. In fact, from the study of hand anatomy and from the analysis of hand behavior during grasping, it is possible to obtain useful information for developing human-like grasping algorithms and for improving knowledge about hand kinematics in order to design anthropomorphic robotic hands endowed with high dexterity and innovative rehabilitation devices. Namely, the definition of hand and finger kinematic structure is one of the most focal points for designing dexterous robotic hands and devices intended for interaction with humans (such as rehabilitation devices).

In the field of robotics for assistance, the ability to realize smooth movements and to obtain a stable grasp is of primary importance. For this reason, one of the aims of the present work has been that of developing a bio-inspired approach for determining both posture and trajectory of the fingers of a robotic hand during the grasping action. To this aim, a thorough study of the human hand behavior during the grasping action has been performed. The evidence makes it clear that such action can be decomposed into three main phases:

- reaching (the hand approaches the object to be grasped);

- pre-shaping (fingers assume the configuration most suitable to ensure a stable grasp);

- grasping (the object is actually grasped).

In order to reduce the complexity of the control that ensures the stability of grasping, it appears convenient to find the better grasping configuration. During the pre-shaping phase, in fact, on the basis of the physical characteristics of the object to be grasped, such as shape and weight, the hand, while approaching the object, assumes the configuration most suitable for seizing. During this phase, the contact points between the fingers and the object allowing a stable grasp are also found, and the trajectory to be followed by the fingers in order to grasp the object in the determined points is planned. Thus, pre-shaping plays a fundamental role in order to guarantee a stable grasp and, for this reason, in this thesis special attention has been paid to the analysis of this phase.

In order to study the grasping action performed by humans, first, an accurate analysis of the literature regarding anatomy, surgery and rehabilitation of the human hand has been performed [14], [15], [16], [17], [18]. Then, in order to verify some of the results presented in the literature [19], [20], [21], [22] and to fill in some gaps regarding, e.g., the behavior of the thumb, various devices for movement analysis have been employed. In particular, different grasping experiments were carried out, by using the following devices:

- the CyberGlove [23], a glove provided with sensors, able to supply the values of the finger joint angles during hand movements;

- the Vicon vision system [24], made of eight infrared TV cameras that supply the positions of a set of markers located on the hand according to a chosen configuration;

- the Kinect® motion sensing system [25], made of two TV cameras, RGB e IR, integrated in a single device.

The hand configuration during grasping depends both on the shape of the object (in an increasing way, as far as the hand approaches the object, reaching a maximum when the hand grasps the object [26]) and on the task to be performed after grasping [27], [28]. Hence, in order to establish the protocol to be followed for executing the experiments, different grasping taxonomies present in the literature have been taken into account [29], [30], [31].
Five experiments on different subjects have been performed with the CyberGlove and the Vicon. The subjects have been asked to grasp, without raising, four objects (a bottle, a sphere, a pen and a CD case) with different types of grasp: force grasp with two different thumb configurations for seizing the bottle, three-digital grasp for seizing the sphere, precision grasp for seizing the pen and, finally, lateral grasp for the CD case. It has been decided to perform these four grasps since they represent the most common grasps executed in the daily life.

The analysis of the data obtained has been mainly centred on power grasp, considering both thumb configurations: transverse volar grasp, where the thumb is opposite to the other fingers, and diagonal volar grasp, where the thumb lies along the rotation axis of the object. The obtained results are interesting and will be illustrated in Chapter 3.

For a more complete analysis of the human hand behaviour, the motion sensing system Kinect has also been used. In this way, it has been possible to perform the triangulation of the visual features necessary for estimating the hand posture. A set of markers has been placed on the hand with the same configuration used for the Vicon and the marker detection during motion was made by using a blob detection algorithm. A crucial problem has been tracking the markers along the image video sequence, taking into account the presence of noise and the possibility that markers appear and disappear during motion. To this end, an algorithm using the theory of Bayesian estimation and suitable filtering techniques has been implemented.

The obtained data have been used for implementing a bio-inspired algorithm for force grasp. The developed approach is based on studies according to which

when a human subject seizes a cylindrical object with a diagonal volar grasp, the best grasping configuration is the one that minimizes the distances between the hand joints and the object surface. From the analysis of the data obtained in the experiments performed, it has been possible to show that the approach can be extended to the transverse volar grasp. The implemented algorithm allows finding the optimal hand configuration for firmly grasping an object of given shape and size. The data obtained about the thumb behaviour made it possible to extend the algorithm to the five fingers. The trajectory followed by fingers for reaching the final position is also planned in such a way to replicate the human behaviour.

The experimental validation of the algorithm on a real arm-hand robotic system, composed of the MIT-Manus robot arm and the DLR-HIT-Hand II, is finally proposed. The results of the experiments, carried out on the Biomedical Robotics and Biomicrosystems Lab at Campus Biomedico (Rome), have proved the feasibility and reliability of the algorithm, as it will be exposed in Chapter 5.

Summarizing, the purposes of this thesis are:

- to find, from the analysis of human grasping behavior, a general rule for performing a stable, human-like cylindrical grasp with a robotic hand;
- to provide the basis for finding an optimal grasp configuration always applicable to certain grasping conditions;
- to propose a new rehabilitation interface for a hand rehabilitation device.

Finding a general rule for obtaining an optimal grasp configuration has the objective:

- to reduce the number of active degrees of freedom (DOFs) strictly necessary for controlling the hand shape (as it has been done with synergies);
- to develop grasp configuration algorithms with reduced computational costs.

Chapter 2

The human hand: Anatomy and kinematic structure

The human hand represents the most dexterous part of the human body, both for its complex mechanical structure and for the versatility of its possible activities. Further it is deeply linked with the brain. Indeed, the communication between the hand and the brain is bidirectional: the hand allows us to feel the surrounding environment by touch, and contributes to the mental processing of feeling. The neuroplasticity concept, at the basis of neurorehabilitation, is based on this bidirectionality: the brain re-learns the motor patterns when the hand repeats predefined movements so that the hand re-learns how to move itself thanks to the brain improvements. Within this sensorimotor continuum, it is possible to identify the following four hand activity categories [32].

- Tactile sensing: it is the situation in which, during the contact between the hand and the object, the hand is always stationary, therefore passive.

- Active haptic sensing: there is the contact between the object and the hand that the subject moves voluntarily over the object surface, and thus the hand is always active.

- Prehension: it is the activity in which the hand reaches the object in order to grasp it. The activity involves also holding the object.

- Non-prehensile skilled movements: the hand gestures used as a part or in substitution of normal speech are included in this activity.

This research is focused on the analysis of the prehension activity since our aim is to propose a bio-inspired grasping algorithm on the basis of the analysis of the human grasping action.

In order to understand the mechanisms behind the human hand movements, an analysis of the anatomy, surgery and rehabilitation literature published over the years has been carried out. It is generally acknowledged that performing a natural and reliable grasp with a robotic hand is a challenging task not yet completely solved. The study of the human hand behavior is the basis for designing a robotic hand as similar as possible to the human one, both from the aesthetical and functional points of view. Particular attention has been paid to the human hand movements involved in daily life activities. In order to identify the most common hand configurations, an analysis of grasp taxonomy has been done. Further, it has been checked whether natural constraints in the human hand structure exist. The introduction of the hand kinematic model is essential for studying the grasping postures. A comparison with the kinematic models commonly used in the robotic hand design has been finally done, outlining the differences with the human one.

2.1 Anatomy of the human hand

In order to deep on the knowledge about the hand grasping behavior, it has been helpful to review the basic structure of the hand, with special regard to bones and joints. The human hand (Fig. 2.1) is made of 27 bones: 8 carpal bones, 5 metacarpal bones in the palm and 14 bones for the digits [33].

Neglecting the palm, the hand joints can be grouped in the following classes:

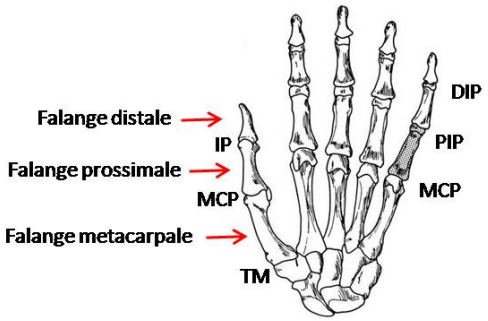

Figure 2.1: Hand mechanical structure

- metacarpo-phalangeal (MCP) joints: characterized by 2 DOFs (adduction/abduction and flexion/extension);
- proximal intra-phalangeal (PIP) joints: 1 DOF for flexion/extension;
- distal intra-phalangeal (DIP) joints: 1 DOF for flexion/extension;
- trapeziometacarpal (TM) joint: it has 2 DOFs, one for adduction/abduction and the other for flexion/extension;
- inter-phalangeal (IP) joint: 1 DOF (flexion/extension).

Furthermore, the long fingers (index, middle, ring and little finger) have 4 DOFs each, the thumb has 5 DOFs and the translational and rotational movements of the palm are characterized by 6 DOFs altogether. Therefore, as a whole, the human hand has got 27 DOFs.

This complex structure gives the human hand extremely dexterous motor capabilities, combining the capacity to perform powerful grasp as well as delicate movements and fine manipulation tasks. Different grasping actions, such as different hand movements, involve a different number of DOFs and thus a different amount of exerted forces. Grasping has been defined as "every static hand posture with which an object can be held securely with one hand". Understanding the human grasping action mechanisms is of primary interest in order to impart those

skills to robotic hands. In order to reduce the complexity of hand control, it is useful to understand whether humans use a combination of basic grasp configurations for prehensile postures. This hypotheses has been confirmed in [34] where it is suggested that a human hand uses combinations of grasps. Behavioral studies have shown that the grasping posture depends on the object physical characteristics (as shape and size), but also from the task to perform once the object has been grasped [35]. The effect of the object shape on the hand configuration gradually increases as the hand approaches the object [26], peaking when the hand grasps the object. By considering only the characteristics of the object the hand interacts with, Schlesinger [36] divided the human hand grasping into six different types of prehension (Fig. 2.2). In this classification the task to be performed is not considered, whilst the choice of the grasp is mainly dictated by the task to be accomplished.

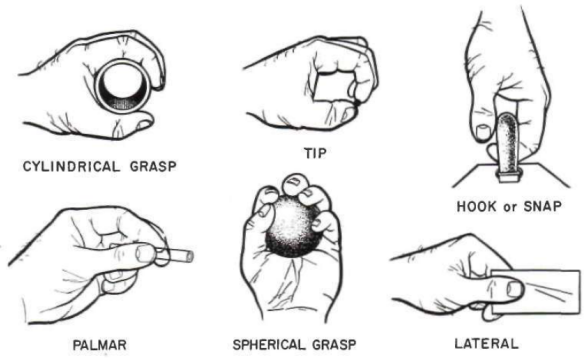

Figure 2.2: Hand grasping taxonomy proposed by Schlesinger [36].

According to the task, some grasping taxonomies have been proposed in the literature [37], [38], [29], [30], [31]. In particular, two principal classes of grasps are distinguishable: power grasp, in which the whole hand is involved, and precision grasp, where only fingers are involved. Among power grasps, the attention has been mainly focused on two types of cylindrical power grasp, discussed in [39]: transverse volar grasp, where the thumb is abducted, and diagonal grasp, where the thumb is adducted lying along the longest axis of the object surface (Fig. 2.3).

(a) Diagonal volar grasp

(b) Transverse volar grasp

Figure 2.3: Power grasp classification proposed by Buchholz.

Cutkosky [40] provided a much more comprehensive and detailed classification of human grasping, proposing a taxonomy tree that starts from the classification done by Napier [31] (power and precision grasps) and extends it by dividing the two types of grasps according to the object shape and task (Fig. 2.4). The drawback of this classification is that it has a large amount of classes, and it is difficult to apply it for defining a collective behavior.

Considering the way in which the hand can apply opposing force around the object for a given task, in [41], three types of prehension are identified (Fig. 2.5): pad opposition (the finger motion direction is parallel to the palm), palm opposition (the finger motion direction is perpendicular to the palm) and side opposition (the thumb is oriented toward the sides of the other fingers). With a combination of these three grasp primitives it is possible to realize each grasp configuration.

It is possible to conclude that, in daily life, some hand configurations are mostly used. Since one of the aims of this research is to apply the obtained results in the field of medical robotics (prostheses, rehabilitation and assistance devices), the attention has been focused on daily life activities. Combining this consideration with the taxonomies found in the literature, five types of grasps have been analyzed. Therefore, our attention has been focused on power grasp (subdivided into lateral and diagonal volar grasp), pinch grasp, lateral grasp and tripod grasp (Fig. 2.6).

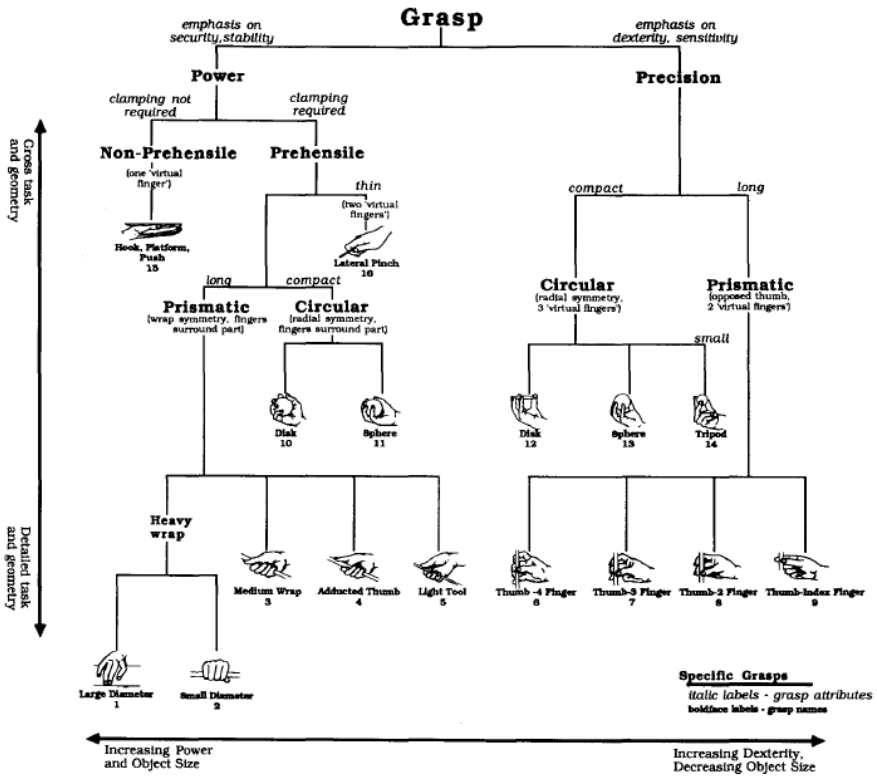

Figure 2.4: Hand grasping taxonomy proposed by Cutkosky [40].

A further simplification in the analysis of the human hand grasping action can be obtained by analyzing the kinematic structure of the hand. In fact, it is possible to note that the hand shows some common behaviors between different subjects, leading to think that the hand joints are mechanically constrained.

2.2 Human hand kinematic model

In order to model the kinematic structure of the human hand, each finger can be modelled by a kinematic chain and the wrist can be considered as the origin of the reference frame. The joint type utilized in the model is chosen on the basis of the DOFs associated to each of them. Since the MCP joints have 2 DOFs, it is

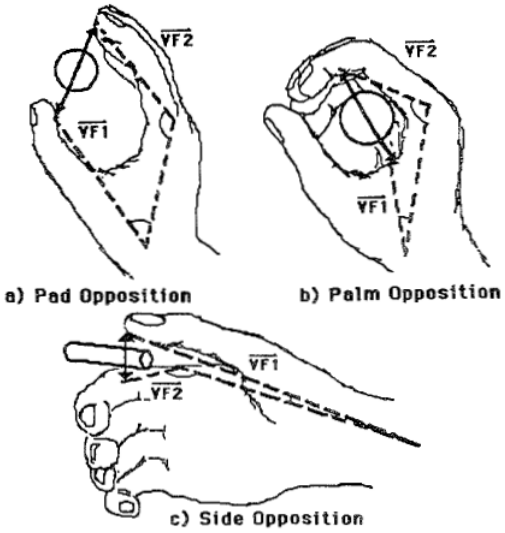

Figure 2.5: Hand grasping taxonomy proposed by Iberall [41].

(a) Diagonal volar grasp

(b) Transverse volar grasp

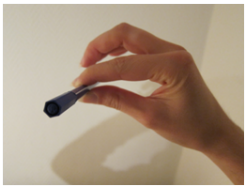

(c) Pinch grasp

(d) Lateral grasp

(e) Tripod grasp

Figure 2.6: Grasp configurations analyzed in this thesis.

convenient to model it as an ellipsoidal joint, that allows flexion/extension as well as limited lateral deviation; since PIP and DIP joints have 1 DOF each, they can be modelled with hinge joints that allow movements in only one direction. The thumb MCP joint is a saddle joint that gives the thumb the ability to cross over the palm of the hand (Fig. 2.7).

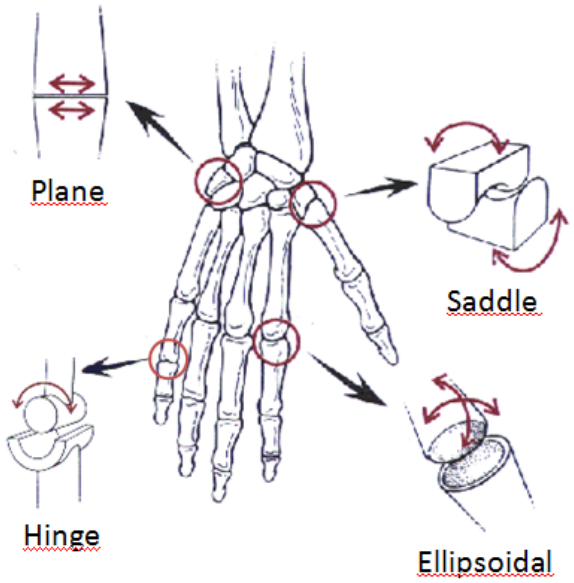

Figure 2.7: Human hand joints.

The most commonly used motion constraints are [22], [42]:

1. On the range of motion of the finger joints due to the hand structure:

$$\begin{cases} 0^o \leq \theta_{MCP_f} \leq 90^o \\ 0^o \leq \theta_{PIP} \leq 110^o \\ 0^o \leq \theta_{DIP} \leq 90^o \\ -15^o \leq \theta_{MCP_a} \leq 15^o \end{cases} \tag{2.1}$$

where MCP_f and MCP_a are referred to flexion and adduction, respectively.

2. On the abduction of the middle finger. It is commonly adopted an approximation of 0 degrees for this angle.

$$\theta_{MCP_a} = 0. \tag{2.2}$$

3. On the correlation among the PIP and DIP joints of the long fingers:

$$\theta_{DIP} = \frac{2}{3}\theta_{PIP}. \tag{2.3}$$

It is possible to find several studies about the identification of a valid hand kinematic model [43], [44], [45], [46], [47] or of a tendon force distribution model [48], [49]. In [50] it has been proved that there is a high correlation between the Trapezio-Metacarpal (TM) and MetaCarpo-Phalangeal (MCP) joint flexion (1^o of flexion at the TM joint implies a flexion of 0.77^o at the MCP joint) and between the flexion and pronation of the TM joint (as flexion increases by 1^o, the pronation increases by 0.90^o). In order to simplify the model of the thumb, it is possible to find some approximations, for example regarding the TM joint, that has a limited abduction motion: $\theta_{TM_a} = 0$. Actually, the thumb TM joint motion includes flexion/extension, addubtion/abduction and pronation/supination. Although the motion occurs in all these three planes, the TM joint is a two-DOF joint: for any position of extension and abduction, there is a set degree of pronation [51]. In [18] a deep analysis of the TM joint of the thumb has been done, outlining that the abduction/adduction axis of this joint forms an angle of 72.7 ± 8.4^o with the flexion/extension axis and that they are not intersecting.

From the above considerations, it is possible to represent the kinematic chain of the human fingers as reported in Fig. 2.8, where, for the sake of clarity, only the thumb and the index finger kinematic chain are shown. The middle, ring and little fingers have the same kinematic chain of the index finger. In this model, it has been supposed that the adduction/abduction movement of the thumb is due essentially to the TM joint, and thus it has been supposed that the MCP joint

has only 1 DOF.

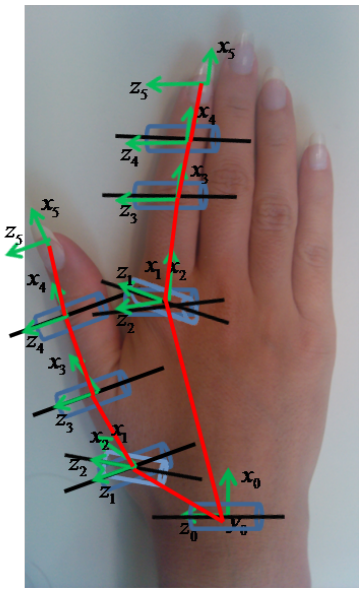

Figure 2.8: Human hand kinematic model. The middle, ring and little fingers have the same kinematic chain of the index finger.

2.3 Robotic hand kinematic model

By analyzing the robotic literature, it is interesting to note a sizeable lack of information about the thumb behavior, despite its fundamental role during the grasping action. Some examples of anthropomorphic hands are:

- The Utah/MIT hand [52]: it is a four-fingered robotic hand developed in 1982 by the Center for Engineering Design of the University of Utah and the Artificial Intelligence Laboratory of the Massachusetts Institute of Technology. The four fingers, each containing four joints, are essentially identical although one of them acts as the thumb. The system is tendon driven. The finger MCP joint is made of two separated joints in order to avoid undesirable two-dimensional deformations of the tendons due to tendon routing

limitations (Fig. 2.9). The axis of the 0 joints in Fig. 2.9 lies parallel to the

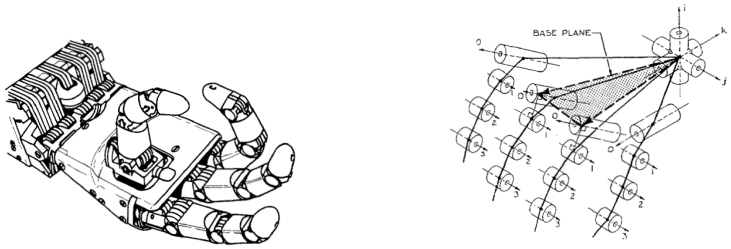

(a) Design of the Utah/MIT hand version III

(b) Utah/MIT hand configuration. The finger joints are shown.

Figure 2.9: The UTAH/MIT hand.

base plane, while in the human hand it is perpendicular to the base plane. Also this configuration is due to tendon routing limitations. Although the base of the thumb is placed on the hand palm, in a non-anthropomorphic configuration, it seems that the thumb can interact with the other fingertips in a quite natural manner. The flexion degrees of all the finger joints (MCP, PIP and DIP, corresponding to joints 1, 2 and 3 respectively in Fig. 2.9) go from 0^o to 95^o. The adduction angle of the thumb goes from -45^o to 45^o, while for the other three fingers it goes from -25^o to 25^o.

- The Anthrobot 2 [53]: It is a five-fingered robotic hand built at NASA Goddard in 1993. The four long fingers have four DOFs as the human hand. Also the thumb has four DOFs: one for each of the IP and MCP joints and two DOFs for the TM joint. The opposition of the thumb is allowed by two pulley-driven links. In the hand, there are 16 servomotors and 20 joints; among them, DIP and PIP joints are coupled 1:1.

- The Robonaut hand (Fig. 2.10) [54]: It is a five-fingered robotic hand developed for the extra vehicular space activities use. It includes the forearm, in which there are the motors, and has a total of 14 DOFs. The hand fingers are different among one other. The index and the middle fingers have

3 DOFs: 2 DOFs for the MCP joint, which have an adduction angle that goes from -25^o to 25^o and a flexion angle of 100^o, and 1 DOF for the PIP and DIP joints, that are coupled 1:1. The ring and the little fingers have one DOF each: the three joints (MCP, PIP and DIP) are coupled 1:1. The thumb has a proximal and distal segment and has 3 DOFs (2 DOFs for the MCP joint). It is mounted on the same side of the long fingers, enabling the hand to perform grasps that are not possible with the hands in which the thumb is opposed to the other fingers (so as for example the UTAH/MIT hand). The thumb MCP joint has 70^o of adduction and 110^o of flexion. The IP joint has 80^o of flexion. The hand uses flex shafts to transmit power from the motors in the forearm to the fingers.

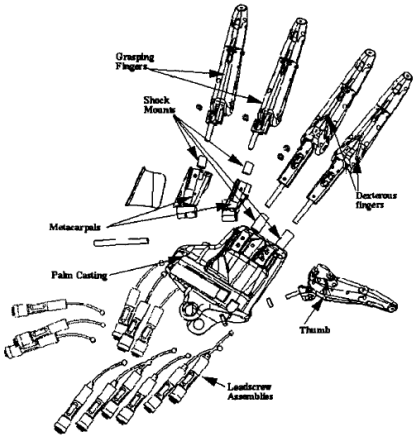

Figure 2.10: The components of the Robonaut hand.

- The DLR-HIT-Hand II [55]: it is a robotic hand with five identical fingers. In [56] the aim is to produce a guideline for obtaining a functional robotic thumb integrated in the DLR robotic hand. A detailed description of this hand, that we used in the experiments, will be given in Chapter 5.

- The UB Hand IV (Fig. 2.11) [57]: it is a robotic hand developed by the University of Bologna in the framework of the Dexmart European Project.

The hand has five identical fingers. Each of them has 4 DOFs: 2 DOFs for the MCP joint, which adduction angle ranges from -10^o to 10^o, and 1 DOF for PIP and DIP joints, which are coupled 1:1. The MCP, PIP and DIP joint flexion angle goes from 0^o to 90^o.

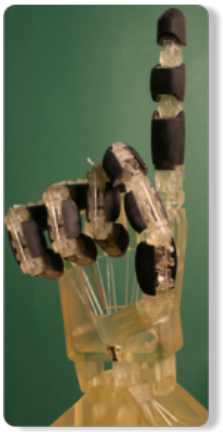

Figure 2.11: The UB hand IV.

It is possible to conclude that developing a robotic hand with the same kinematic characteristics of a human hand has not yet been achieved. In fact, the robotic hands designed until now are not able to replicate the motor capabilities of the human hand. In order to give some hints for improving the robotic hands realized until now, in the following chapters it will be shown that it is possible to find some grasping features that are common for all the human beings. Finding some general behavior rules in the grasping action may allow the robotic hand designer to reduce the complexity of the hand control by decreasing the number of active DOFs of the hand.

Chapter 3

Experimental analysis of the grasping action performed by a human being

In Chapter 2, some approaches attempting to understand the behavior of the human hand during grasping have been reported.

However, by analyzing the robotic literature, it is interesting to note a sizeable lack of information about the thumb behavior, despite its fundamental role during the grasping action. Actually, as previously said, it is possible to find several studies about the identification of a valid hand kinematic model, but adequate information about the thumb behavior, mainly regarding the analysis of its functional aspects, is lacking.

In order to understand the human grasping behavior and to measure the Range of Motion (ROM) [20], [58], [59] of the fingers, different techniques can be used, e.g. goniometers [60], ultrasound [61], virtual glove, marker-based motion capture [50], [62], [63], [64], [65].

With the aim of confirming some of the results illustrated in the literature and to overcome some lacks regarding, e.g., the thumb behavior, in this chapter some grasping experiments performed with two different motion analysis devices will

be presented. The used devices are:

- the CyberGlove, a data glove equipped with 22 sensors;
- the Vicon system, a 7-camera optical system.

3.1 CyberGlove

In the literature some discussions can be found about tests made for assessing accuracy (in terms of error in recognizing joint angles), resolution, repeatability and linearity of the CyberGlove^{TM} [23] showing the goodness of the measures taken with this hand input device. In the experiments illustrated in this section a CyberGlove has been used for getting information about the thumb behavior during the four fundamental grasps introduced in Chapter 2. The data acquisition has concerned with all those four type of grasps, but the data analysis has been limited, for the moment, to the grasp of cylindrical objects.

The CyberGlove motion capture data glove (Virtual Technologies, Palo Alto, CA) is fully instrumented with 22 resistive bend sensors that measure the five finger joint angles. In Fig. 3.1, the positions of the Cyberglove sensors are outlined with yellow circles, while the corresponding measured angles are listed in Tab. 3.1.

The sensors are thin, flexible and have a resolution less than one degree. They are so located:

- three flexion sensors per finger,
- four abduction sensors,
- one palm-arch sensor,
- two sensors for measuring wrist flexion and abduction.

The data glove uses resistive bend-sensing technology to accurately transform hand and finger motions into real-time digital joint-angle data. The sampling frequency used by the CyberGlove is 30 Hz.

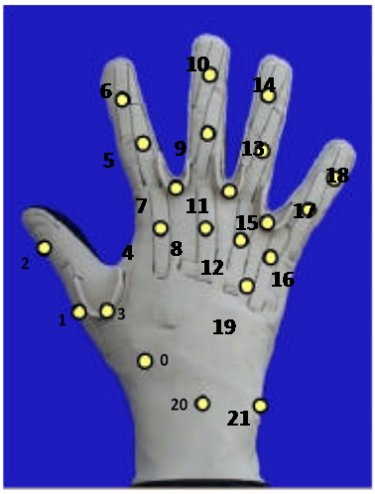

Figure 3.1: CyberGlove with joint sensor locations outlined with yellow circles.

3.1.1 Experimental setup

Ten human subjects, 22.4 years old on the average (1.5 Standard Deviation), all men and right handed, have been asked to grasp four objects with four different types of grasp (Fig. 3.2):

- a bottle with a transverse volar grasp,
- a ball with a tripod grasp,
- a pen with a pinch grasp,
- a CD case with a lateral grasp.

Subjects have woren a 22 sensorized CyberGlove for the right hand, and have been asked to grasp the objects for 10 times each.

The participants have been seated in front of a table on which the objects have been located in a-priori known positions. Hand starting position and initial posture have been the same for all the participants (Fig. 3.3): the shoulder has been abducted of 0^o in the frontal plane and flexed of 0^o in the sagittal plane. The elbow has been flexed with an angle of 90^o in the sagittal plane. The wrist has

Table 3.1: Measured angles from the CyberGlove sensors.

Sensor #	Measured angle
0	Thumb roll sensor
1	Thumb inner joint sensor
2	Thumb outer joint sensor
3	Thumb-index abduction sensor
4	Index finger inner joint sensor
5	Index finger middle joint sensor
6	Index finger outer joint sensor
7	Index-middle abduction sensor
8	Middle finger inner joint sensor
9	Middle finger middle joint sensor
10	Middle finger outer joint sensor
11	Middle-ring abduction sensor
12	Ring finger inner joint sensor
13	Ring finger middle joint sensor
14	Ring finger outer joint sensor
15	Ring-little abduction sensor
16	Little finger inner joint sensor
17	Little finger middle joint sensor
18	Little finger outer joint sensor
19	Palm arch sensor
20	Wrist flexion sensor
21	Wrist abduction sensor

been in a neutral position with 0^o for flexion/extension and 0^o for the radio-ulnar deviation. The forearm has been in the so called mid-prone position with the palm perpendicular to the transverse plane. The object has been at a distance of 53 cm from the sensor on the wrist and the starting hand configuration has been the one in which the four fingers are fully extended and the thumb is adducted. The

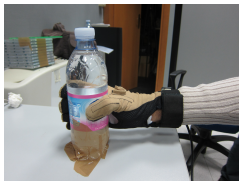

(a) Transverse volar grasp

(b) Tripod grasp

(c) Pinch grasp

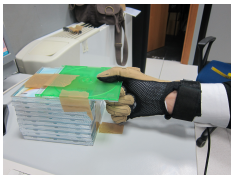

(d) Lateral grasp

Figure 3.2: Grasp configuration obtained with the CyberGlove.

hand joint angles have been recorded in this starting position and in the position in which the hand is completely closed around the objects.

Figure 3.3: Staring position of the subjects with respect to the table on which the objects have been located.

Every subject has been asked to grasp the object, without lifting it, ten times. The data acquisition of each trial has started with a voice command. After grasping the object, the subject have remained in this grasping position until an auditory signal announcing the acquisition end. Before starting the data acquisition, each participant has been asked to grasp the object five times, for learning the grasping action.

After completing the test, the lengths of each finger segment (distal, medial, proximal phalanx and metacarpal phalanx of the thumb) of each subject has been measured with a caliber. Lengths have been measured as the distances between the two extreme bones of the link. These data have been used for constructing the hand direct kinematic.

Since one of the aim of this thesis is to present the integration of the results on human behavior during power grasp, obtained with the CyberGlove motion analysis system, with a bio-inspired optimization algorithm for hand posture prediction, only the data about the power grasp will be analysed. One of the future possible activities will be to extend the investigation to the other three types of grasps.

3.1.2 Data analysis

Since the CyberGlove has to be manually calibrated for each subject, the starting angles could be different among the subjects. However, all the subjects have been asked to start the grasping action with the hand fully opened, thus it is reasonable to expect having small values for the starting angles. In any case, in order to analyze the data, it has been chosen to subtract the angle values obtained in the first frame (hand in the rest pose) from the angle values obtained in the last frame (object grabbed). The angle values that will be considered in the rest of this section will be these difference values. In this way, we have expected to make the final values of the angles independent of those in the initial configuration, obtaining to virtually realize the initial condition of zero starting angles.

In order to understand if it exists a common behavior among subjects during the grasping action, a statistical analysis on the CyberGlove data has been carried out. Since our main aim is to find information about the thumb behavior during grasping, the values supplied by the sensors on the thumb and the index finger have been considered. One of the performance parameters we have been interested in is the aperture angle, computed as the angle between the link connecting the MCP joint of the thumb and the wrist and the link connecting the MCP joint of

the index finger and the wrist. This parameter is useful for having information about the position of the thumb during grasping and can be evaluated once a kinematic model of the hand has been adopted.

The modelling of the hand joints has been made by merging information about the joint axis of rotation taken from the literature [43], [44], [59] (as explained in Chapter 2) and the joint angle values given by the Cyberglove sensors. The MCP and IP joints of the thumb and the PIP and DIP joints of the index have been modelled as a hinge joint with 1 DOF. The TM joint of the thumb and the MCP joint of the index finger have been modelled as ellipsoidal joints with perpendicular rotational axis and 2 DOFs. The center of the root coordinate system is the center of the wrist (Fig. 3.4). In the kinematic model shown in figure 3.4, the flexion/extension axis of the TM joint has been considered perpendicular to the adduction/abduction axis. Although in the human hand these two axes are inclined of about 73^o, it has been chosen to maintain their orthogonality for computation purposes and for better matching the positions of the CyberGlove sensors.

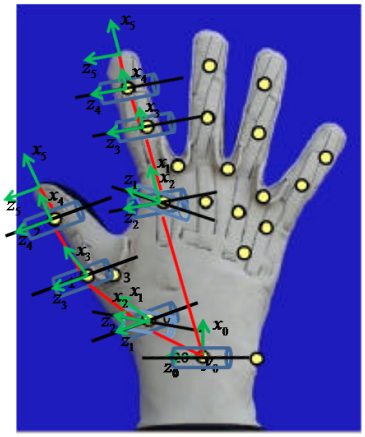

Figure 3.4: Hand kinematic model.

.

The Denavit-Hartenberg parameters for the index finger and for the thumb

are shown respectively in Tabs. 3.2 and 3.3.

Table 3.2: Denavit-Hartenberg parameters of the index finger.

Link #	d	θ	$a\,[m]$	α
1	$d_{1_{index}}$	θ_1	Mc	$-\frac{\pi}{2}$
2	0	θ_2	0	$\frac{\pi}{2}$
3	0	θ_3	P_{index}	0
4	0	θ_4	M_{index}	0
5	0	θ_5	D_{index}	0

Table 3.3: Denavit-Hartenberg parameters of the thumb

Link #	d	θ	$a\,[m]$	α
1	$d_{1_{thumb}}$	θ_1	Tm	0
2	$d_{2_{thumb}}$	θ_2	P_{thumb}	$-\frac{\pi}{2}$
3	0	θ_3	0	$\frac{\pi}{2}$
4	0	θ_4	M_{thumb}	0
5	0	θ_5	D_{thumb}	0

3.1.3 Obtained results

Figure 3.5 shows the angle values, measured by the glove sensors positioned on the thumb and the index finger. For each sensor in the x-axis and y-axis the trial number and the joint angle value, expressed in degrees, are respectively reported. The behavior of different subjects is shown by lines of different colors.

From Fig. 3.5 it is evident that the same subject has substantially the same behavior during the ten trials. Different subjects exhibit a variation that goes from 10 to 40 degrees. This variation is present also when analyzing the starting position of the grasping action, due to an imperfect glove calibration. Therefore, despite we have considered difference values, as explained at the beginning of Section 3.1.2, different values in the measured angles are understandable. In order

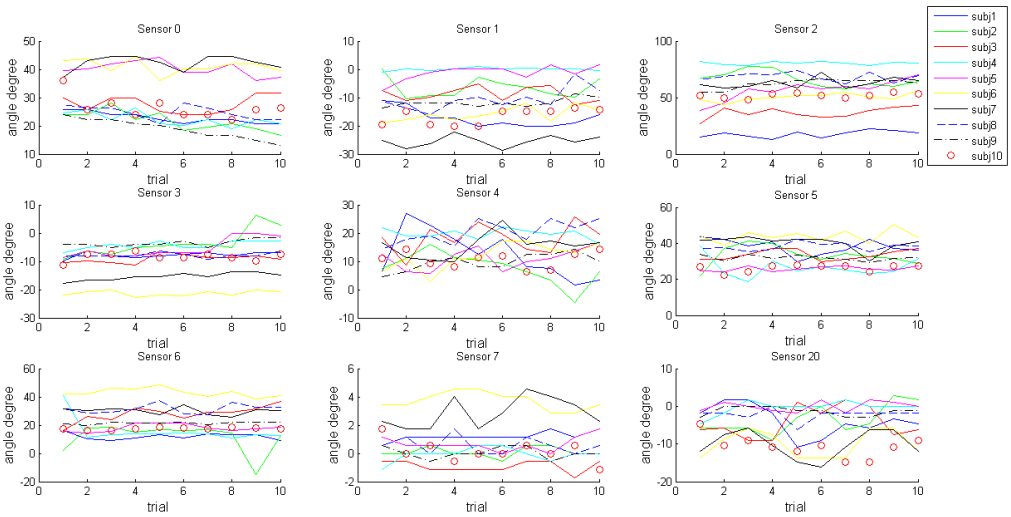

Figure 3.5: Angles measured by sensors on the thumb and the index finger during the 10 trials for the 10 subjects.

to be released from the angle values problem, and to obtain values independent of the initial calibration, the kinematic model introduced above has been used for determining the hand joint positions. From the obtained positions, the aperture angle has been computed. In Tab. 3.4 the mean and standard deviation of the hand aperture angle during the 10 trials are listed.

From the table it is possible to note a quite invariant behavior among subjects for the transverse volar grasp. This consideration might lead formulating a general rule about the thumb configuration during this type of grasp, which could be applied to the grasping algorithm explained in Chapter 5.

However, the joint positions obtained in the above mentioned way, mainly because of the manual calibration of the CyberGlove, do not seem precise enough to control a dexterous robot hand. Therefore it has been decided to use a different motion analysis system assuring better performance as regards data reliability. An optical system based on markers (the Vicon system) has been chosen. The advantage with respect to using a data-glove is the possibility of adapting the

Table 3.4: Mean and standard deviation of hand aperture angle in transverse volar grasp.

Subject #	Mean	SDV
1	48.93^o	0.67^o
2	46.56^o	1.32^o
3	48.90^o	0.51^o
4	47.07^o	0.35^o
5	47.42^o	1.21^o
6	52.36^o	1.73^o
7	51.14^o	1.84^o
8	48.29^o	0.54^o
9	46.58^o	0.82^o
10	48.75^o	0.48^o

marker position to hands of different size, thus enabling the generalization of results independently of subject hand size. Moreover, the system does not need a calibration for each subject. In order to obtain measurements useful for our aims, a critical aspect has been the choice of a protocol for positioning markers on the hand. In the literature, different protocols have been adopted in order to analyze the hand movements, trying to overcome the following problems:

- marker occlusion due by other parts of the hand;
- skin movement, that affects an accurate measurement of joint angles;
- errors in captured marker positions.

In [66] six markers have been attached on each finger, one on the TIP, one on the DIP, two distal and proximal to each PIP and MCP joint (see Fig. 3.6). In [63], three non-collinear markers forming a triangle, are posed on the proximal and medial phalanx in order to determine the joint center near which the markers are applied. In [62] seventeen markers of 6 mm of diameter are placed

in correspondence of the hand joints, as shown in Fig. 3.7. In [64], a protocol for modelling wrist and fingers, including the thumb, trying to assure a repeatable marker placements is proposed. 26 markers of 3 mm of diameter are applied as shown in Fig. 3.8.

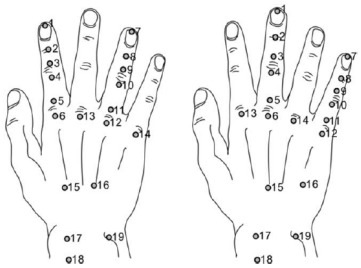

Figure 3.6: Marker placement protocol used by Su et al.

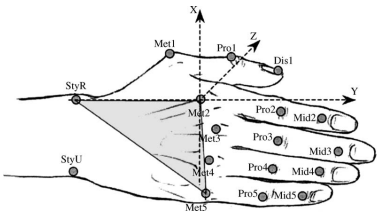

Figure 3.7: Marker placement protocol used by Carpinella et al.

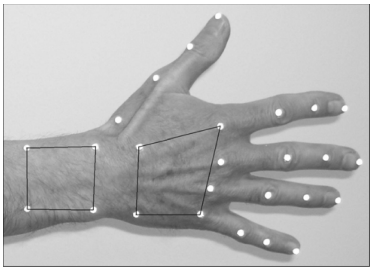

Figure 3.8: Marker placement protocol used by Metcalf et al.

According to the literature results and in order to minimize artefacts, due for example to skin movements or marker occlusions, so as to obtain information

about the wrist position (a reference point for the grasping algorithm, as it will be clarified in Chapter 5), the protocol for positioning markers on the hand shown in Fig. 3.9 has been chosen. The reference frame is positioned on the top of the palm and the marker CMC4 gives information about the palm arch.

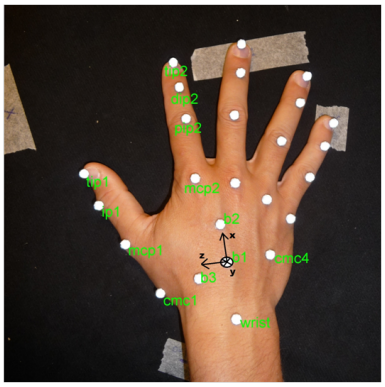

Figure 3.9: Marker configuration with reference frame outlined.

3.2 The Vicon system

The Vicon optoelectronic motion analysis system has been used for collecting information about the thumb and fingers during grasping. The system is composed by 7 InfraRed (IR) cameras, with a frame rate of 100 Hz. It tracks the position of reflective markers in the space, locating their center and calculating their radius. Combining the information from all the cameras, the system fits a circle around the marker image.

3.2.1 Experimental setup

Seven human subjects, 31.7 years old on the average (8.75 Standard Deviation), five men and two women, all right handed, have volunteered to participate in this study. Subjects have been asked to grasp four objects (a cylindrical object of 6 cm diameter, a ball, a pen, a rule), for 10 times each, with the four grasp

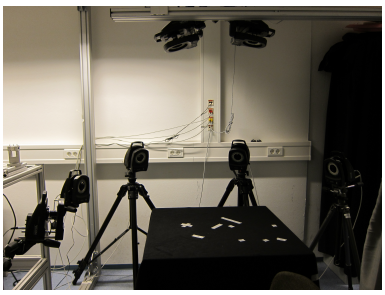

Figure 3.10: Disposition of the cameras with respect the table on which the objects have been positioned.

configurations illustrated with reference to the experiments with the CyberGlove. Further, they have been asked to grasp the cylindrical object also with a diagonal volar grasp, always for ten times. The objects have been covered by paper tape in order eliminate the artefacts due to their cover material (Fig. 3.11).

The Vicon 7-camera motion analysis system has been used to capture data from all the trials; 25 reflective markers of 6 mm diameter have been placed on the subject right hand as shown in Fig. 3.9. All subjects have given informed consent to participate in the study.

Before starting the trials, hand joint ROMs have been recorded asking the subjects to perform some predefined movements. This information has been used during data processing for determining the center of rotation of each joint.

The participants starting position has been the same as for the subjects involved in the experiments with the CyberGlove, with a difference regarding the wrist inclination, which is 45^o with respect to the transverse plane. In order to ensure this inclination, a plastic support has been used for the rest position (Fig. 3.12). This inclination has been necessary in order to ensure a complete visibility of the markers (in particular of the reference frame) in the first frame of the grasping trials.

The hand starting configuration has been the one in which the four fingers are fully extended and the thumb is adducted. The marker positions have been recorded in this starting position and during all the trial until the hand grasps

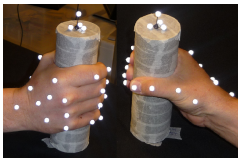

(a) Transverse volar grasp. The thumb positions is outlined in the picture on the right.

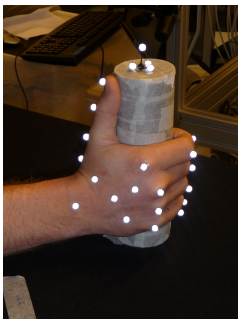

(b) Diagonal volar grasp

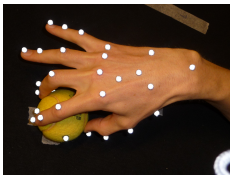

(c) Tripod grasp

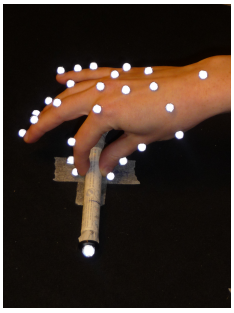

(d) Pinch grasp

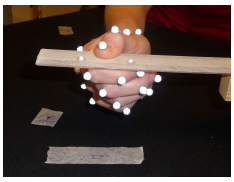

(e) Lateral grasp

Figure 3.11: Grasp configurations obtained with the CyberGlove.

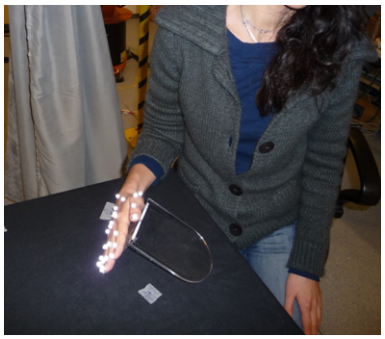

Figure 3.12: Subject starting position.

the object. The object position has been identified by 4 markers placed on the top of the bottle, as shown in Fig. 3.13. Every subject has been asked to grasp the object, without lifting it, ten times. After grasping the object, the subject has remained in this grasping position until an auditory signal announcing the acquisition end. Before starting the data acquisition, each participant has been asked to grasp the object five times, for learning the grasping action.

Figure 3.13: The markers on the object allow identifying its position.

3.2.2 Data analysis

For the analysis of the data, as in this case of the CyberGlove, particular attention has been paid to power grasps.

The Vicon Nexus 1.6.1 software package has been used to reconstruct marker Cartesian positions with the Vicon system and a link model of the hand has been constructed (Fig. 3.14).

In order to understand whether a common behavior among subjects could be observed during the grasping action, a set of performance parameters have been extracted from the data collected with the Vicon system. They are listed in the following.

- The aperture angle of the hand: it is calculated as the angle between the link connecting the MCP joint of the thumb and the wrist and the link connecting the MCP joint of the index finger and the wrist.

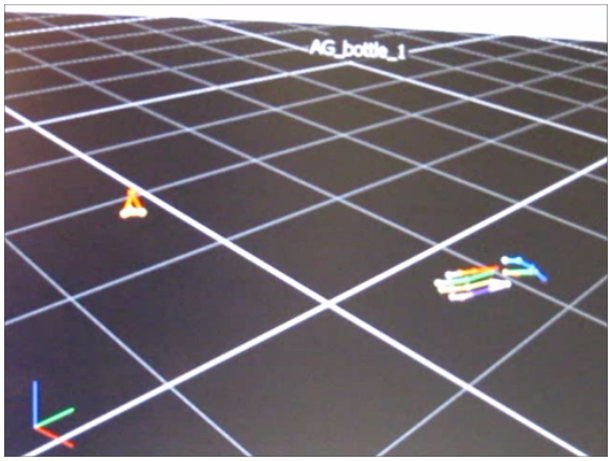

Figure 3.14: Reconstructed marker configuration with the Vicon Nexus software.

- The radius of curvature of every finger: it is the radius of the obsculator circles tangent, at each joint, the spline passing throughout the finger joints.
- The adduction/abduction angle between the fingers: it is the angle between two adjacent fingers and it is subtended by the distance between the PIP joints of the two fingers.
- The thumb opposition angle.

In order to compute the thumb opposition angle, two components have been considered:

- the angle between the x-axis and the projection of the link connecting the MCP joint of the index finger and the CMC1 joint of the thumb onto the xy-plane (Fig. 3.9);
- the angle between the projection of the link connecting the CMC1 and the MCP1 thumb joints onto the z-axis and the link itself.

For computing the above mentioned parameters, the last frame of each trial has been considered for each subject, corresponding to 250 positions (e.g. 10 trials for

25 markers). They are expected to provide useful information about the configuration of all the fingers during grasping. In fact, the first two parameters are useful for obtaining information about the position of the thumb during grasping; the second and the third parameters make it possible to verify also the relation between the long fingers behavior during diagonal volar grasp and transverse volar grasp; the fourth parameter is used for assessing experimental results on the robotic hand and compare them with the human case (as described in Chapter 5).

3.2.3 Obtained results

Figure 3.15 shows the curvature of all the fingers when they are grasping the cylindrical object with a diagonal volar grasp (Fig. 3.15a) and a transverse volar grasp (Fig. 3.15b), respectively. The blue lines are the splines passing throughout the hand joints outlined with different colors, as explained in the figure legend. Furthermore, in Tab. 3.5 the mean and standard deviation of finger curvature radii during a transverse volar grasp and a diagonal volar grasp are listed. The mean is calculated for each subject during the 10 trials. It can be observed a very similar behavior, for the same subject, between the two types of grasp. In Tab. 3.5 only the behavior of the index finger is reported, for brevity, but the results are similar also for the other long fingers.

This finding allows us to extend the grasping algorithm that will be illustrated in Chapter 5 from the diagonal volar grasp to the transverse volar grasp. In other words, it can be concluded that one subject grasps the cylindrical object with the same finger curvature independently of the type of grasp (diagonal or transverse).

In Tab. 3.6 the mean and standard deviation of hand aperture angle during the 10 trials are listed for the diagonal and the transverse volar grasp. From these values, it is possible to note a quite invariant behavior among subjects, for the same type of grasp. This consideration makes it possible to advance a general rule about the thumb configuration during the two types of grasp. This rule has been applied for developing the grasping algorithm explained in Chapter 5.

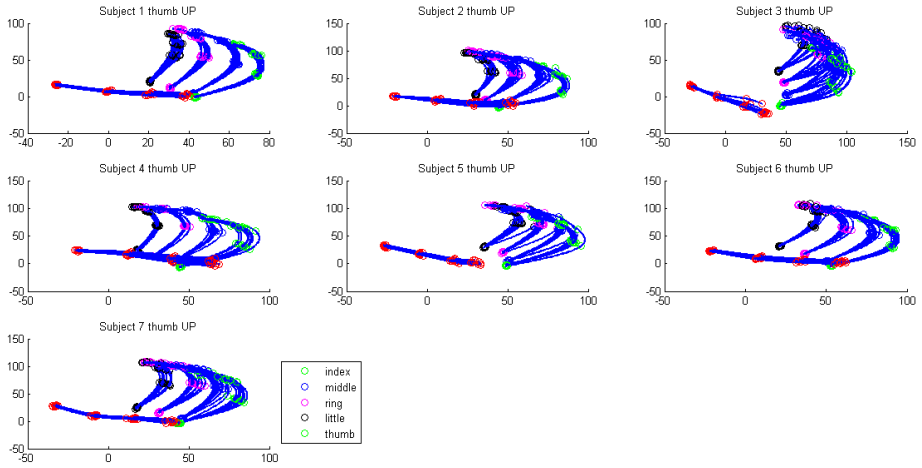

(a) Diagonal volar grasp

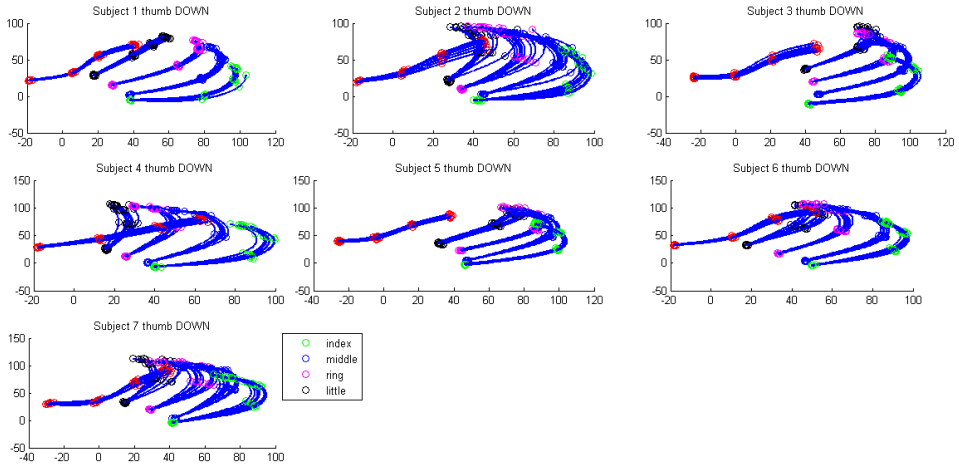

(b) Transverse volar grasp

Figure 3.15: Curvature of the long fingers during diagonal and transverse volar grasps

Table 3.5: Mean and standard deviation of radius of curvature in transverse and diagonal volar grasp for the index finger.

Joint name	Subject #	Diagonal volar grasp		Transverse volar grasp	
		Mean (mm)	SDV	Mean (mm)	SDV
MCP	1	$7.99 * 10^{16}$	$4.48 * 10^{16}$	$8.86 * 10^{16}$	$1.14 * 10^{17}$
	2	$3.81 * 10^{16}$	$2.51 * 10^{16}$	$1.87 * 10^{17}$	$2.25 * 10^{17}$
	3	$3.78 * 10^{16}$	$2.04 * 10^{16}$	$1.07 * 10^{17}$	$6.25 * 10^{16}$
	4	$1.44 * 10^{17}$	$2.71 * 10^{17}$	$6.93 * 10^{16}$	$5.60 * 10^{16}$
	5	$8.31 * 10^{16}$	$7.66 * 10^{16}$	$6.98 * 10^{16}$	$3.46 * 10^{16}$
	6	$9.93 * 10^{16}$	$7.67 * 10^{16}$	$6.77 * 10^{16}$	$6.56 * 10^{16}$
	7	$1.36 * 10^{17}$	$2.03 * 10^{17}$	$7.98 * 10^{16}$	$5.20 * 10^{16}$
PIP	1	28.96	3.01	32.31	2.06
	2	22.81	0.93	26.02	2.51
	3	45.32	1.97	31.99	2.17
	4	33.54	2.32	28.17	1.13
	5	29.10	1.27	26.49	1.13
	6	29.80	1.66	28.36	2.54
	7	31.98	3.51	29.01	1.60
DIP	1	32.83	5.34	29.76	1.75
	2	50.97	8.30	40.84	3.89
	3	26.36	1.48	28.32	2.82
	4	27.19	2.44	34.19	7.82
	5	36.35	4.23	33.03	3.12
	6	44.06	4.22	38.68	5.76
	7	30.95	2.64	27.41	2.30
TIP	1	$6.33 * 10^{16}$	$7.49 * 10^{16}$	$1.04 * 10^{17}$	$1.01 * 10^{17}$
	2	$1.99 * 10^{17}$	$3.02 * 10^{17}$	$1.60 * 10^{17}$	$1.23 * 10^{17}$
	3	$8.08 * 10^{16}$	$9.22 * 10^{16}$	$9.83 * 10^{16}$	$9.80 * 10^{16}$
	4	$1.04 * 10^{17}$	$6.35 * 10^{16}$	$1.08 * 10^{17}$	$1.17 * 10^{17}$
	5	$1.12 * 10^{17}$	$1.34 * 10^{17}$	$6.87 * 10^{16}$	$4.41 * 10^{16}$
	6	$8.52 * 10^{16}$	$6.00 * 10^{16}$	$7.91 * 10^{16}$	$5.14 * 10^{16}$
	7	$1.01 * 10^{17}$	$1.09 * 10^{17}$	$9.14 * 10^{16}$	$9.94 * 10^{16}$

Table 3.6: Mean and standard deviation of hand aperture angle in transverse and diagonal volar grasp.

	Diagonal volar grasp		Transverse volar grasp	
Subject #	Mean	SDV	Mean	SDV
1	49.54^o	1.39^o	51.60^o	0.56^o
2	48.68^o	1.61^o	58.27^o	1.54^o
3	50.39^o	1.22^o	53.13^o	0.42^o
4	56.83^o	1.91^o	52.39^o	4.90^o
5	56.77^o	2.13^o	58.67^o	1.11^o
6	51.56^o	1.30^o	59.06^o	0.38^o
7	53.57^o	0.68^o	59.43^o	1.48^o

Chapter 4

Analysis of hand movements by the Kinect motion sensing device

As said in the previous chapters, reproducing realistic and natural hand movements is a challenging task for robot hand control. In order to understand the human hand behaviour, in Chapter 3 two motion analysis devices have been introduced: the CyberGlove and the Vicon system. However, their use suffers from some drawbacks:

- The Cyberglove is a data glove where the positions of the integrated sensors are fixed; moreover, it can be used only by people of given hand size.
- The movements performed wearing a data glove are not completely natural since the glove limits the hand movements.
- The CyberGlove needs a calibration for each subject.
- The Vicon motion analysis system is quite expensive, and thus the experiments with it are not easily repeatable everywhere.

In order to overcome these drawbacks, and to obtain information about the hand movements, the Kinect motion sensing device, developed by Microsoft, has

also been used. In this way, it is possible to realize the visual analysis of human hand motion, and to record the hand joint positions during movements in a reliable and repeatable way. The system is very cheap and facilitates the triangulation process of the visual features, fundamental for hand pose estimation.

In this chapter, a short description of the technology on the basis of which the Kinect works is first provided. Then, the literature approaches for solving the problem of finger tracking are introduced and our solution is illustrated. Finally the application of the developed algorithm in the field of graphic interfaces for hand rehabilitation devices is presented.

4.1 The Kinect motion sensing device

The Kinect (Figure 4.1) is a motion sensing device consisting of an InfraRed (IR) laser emitter, an IR camera, for measuring depth information, and a RGB camera. It captures depth and color images simultaneously at a frame rate of about 30 frames per second (fps). The resolution of the RGB camera is 640x480. The IR camera and the IR emitter form a stereo pair.

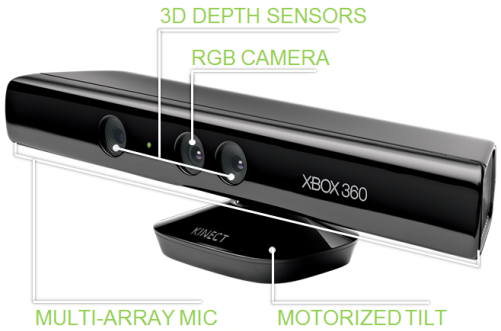

Figure 4.1: The Kinect motion sensing device.

Depth is evaluated by using a CMOS sensor device, produced by PrimeSense, which is not capable to extract the time of return from the modulated light. This is why the Kinect depth sensor does not work using the time-of-flight method, but

using the light coding method. The gestural control systems are usually based on the first mentioned method, according to which the depth information is given by the time the IR light takes to return back to the cameras. The technique on which the Kinect depth sensing system is based [67] requires that two images are compared for the purpose of a triangulation. The IR emitter sends out a single beam which is split by a diffraction grating into a pattern of speckles that is projected onto the scene. This pattern is acquired by the IR camera and is correlated with a reference pattern, already stored, obtained by projecting the same pattern of speckles on a plane, parallel to the depth camera plane and placed at a known distance from the sensor. The result of the correlation procedure between the reference pattern and the speckle pattern projected on an object in the scene is a so-called disparity image. The distance of each object pixel from the sensor can be retrieved by triangulation from the corresponding disparity, on the basis of a simple depth-disparity relation. In the Kinect, the disparity is stored in a 11-bit variable.

The device feature of supplying depth measurements of images formed by the RGB camera can be exploited under the condition that an appropriate calibration of the vision system is made.

Since the Kinect is a motion sensing device marketed by Microsoft for the Xbox 360 video game console, in order to work with it on a PC, it has been necessary to use some suitable libraries, such as LibFreenect by OpenKinect.

4.2 Finger tracking

The visual analysis of human hand motion attempts to detect and track hand movements from image sequences. Hand tracking has several applications: it can allow us to control a teleoperated anthropomorphic robotic hand [68], it could have interesting applications in gesture recognition [69], it could be adopted in order to create a natural interface device [70], it could be used in Virtual Reality, in the field of rehabilitation [4] and so on. The problems to deal with are essentially due

to the segmentation of the hand from the background and to the large number of hand DOFs.

Skin color offers a possible way for locating the hand in image sequences. In this case, the hand could be identified as a unique coloured blob making difficult the identification of finger motion. Therefore it is necessary to extract some features, as points, contours, silhouettes, [71] to be tracked. The human hand is characterized by a high number of DOFs. The approaches generally used for tracking this type of objects are of two types [72]:

- the appearance-based approach: in which 2D deformable hand templates are used to track a hand in 2D. Therefore, this method is not enough for recovering full articulations [73].

- the 3D model based approach: that estimates articulated motions by projecting a 3D model on to the image space and then compares the projections with the observations. The best matching between the image feature observations and the projected 3D model gives the joint angle values. Therefore, this problem has been formulated as an optimization problem [74], [75].

The last approach has a high computational cost since the searching space has a very high dimension. In order to simplify the optimization, it is possible to incorporate in the hand model some constraints, based on the natural movements of the hand [76]. In order to solve the optimization problem, sequential MonteCarlo methods, such as particle filters, have been used [77], [78], [79], [80].

Combining the characteristics of the described approaches and adapting them to our case, the following approach for tracking the hand joints has been developed.

4.2.1 Hand joint tracking algorithm

In order to obtain information about the hand joint positions during motion, coloured markers have been located on a human hand, in the same configuration used with the Vicon system (Fig. 4.2). The markers have been realized by using

pieces of paper, of diameter 1.2 cm, consisting of a central blue circle surrounded by a white ring. This external white part has revealed to be useful in order to make the detection algorithm robust when finger projections overlap among each other.

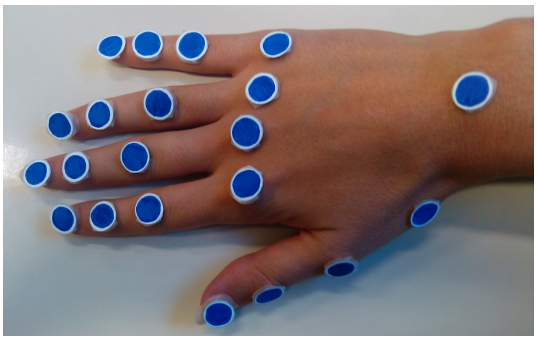

Figure 4.2: Protocol used for marker positioning.

Marker detection and tracking are the core problems in reconstructing the hand joint positions during hand movements: in the following a detailed overview of the techniques used to detect and track the projection of finger joints on successive images is given. In this work the perspective camera model (Fig. 4.3 [81]) is used, which corresponds to the ideal pinhole camera model.

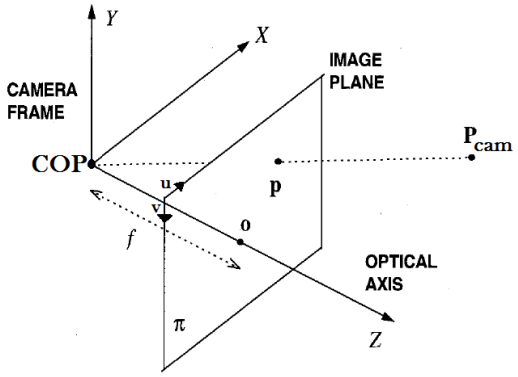

Figure 4.3: Perspetive camera model.

The model consists of the image plane π, and a point called center of projection

(COP). In Fig. 4.3, f is the focal lenght, i.e. the distance between the image plane and the COP; the optical axis is the line passing through the plane π and the COP; the point o is the principal point (also called image center), i.e. the point where the line from the camera center, perpendicular to the image plane, meets the image plane itself. Once the COP and an image plane have been chosen, the projection problem is fully determined [82]. Thus, the projection p of a point in the 3D space $P_{cam} = \begin{bmatrix} x & y & z \end{bmatrix}^T$, relative to the camera coordinates, is obtained as the intersection of a line passing through this point and the COP with the image (retinal) plane, that is, by using homogeneous coordinates:

$$\begin{bmatrix} u \\ v \\ 1 \end{bmatrix} = \begin{bmatrix} f_x & 0 & c_x \\ 0 & f_y & c_y \\ 0 & 0 & 1 \end{bmatrix} \begin{bmatrix} \frac{x}{z} \\ \frac{y}{z} \\ 1 \end{bmatrix} \tag{4.1}$$

where u, v are the pixel coordinates of the projection of the scene point P_{cam} onto the image plane; f_x, f_y are the focal lengths and c_x, c_y are the coordinates of the principal point. The two sets of parameters are expressed along the x and y directions of the camera reference plane and they are called intrinsic camera parameters.

4.2.2 Detection

Aim of the feature detection process is to extract useful information from images (abstraction of images) allowing us to decide whether a certain image point is an image feature of a given class or not. Generally speaking, a feature is a characteristic or a part of an image which brings a certain type of information about the scene. Since the concept of feature is "case dependent" and not unique, a high number of features could be extracted, given one image, i.e. corners, edges, region of interests/blobs, and so on. Corners and edges are useful to solve the detection problem in such frameworks where the structure of the observed scene is not a priori known, that is no a priori information about the scene is available.

On the other hand, Regions Of Interests (ROIs) provide a complementary description of image structures in terms of regions, and they are recommended when the information to be extracted from images belong to a certain and known class, which can be expressed in terms of coloured regions, patterns, and so on. Since in the hand pose reconstruction the projection of the markers attached to the hand joints is the only interesting part, it is evident that the ROI concept is the one which better allows the solving the detection problem at hand, whose objective is the identification of image areas associated with the targets. The approach followed in this thesis aims at detecting the coloured markers within the input video, for each frame. Therefore, it has been chosen to look for those regions of connected pixels, within the image, whose histogram is as close as possible (in the sense of Bhattacharyya similarity coefficient) to the reference color histogram (i.e. blue histogram, since blue markers were employed). In order to improve and speed up the extraction process, the image has been thresholded so as to obtain a binary image where the regions, whose histogram is closer to the reference one, are represented by white pixels. Then, a connected component labeling algorithm has been used. In order to identify connected components (a blob is defined as a group of connected pixels), the image has been scanned by rows reading the gray level of each pixel. If the gray level of a pixel exceeds the given threshold (i.e., the pixel is identified as a white pixel), its position is stored, since it is possible that such pixel belongs to a candidate blob. The above procedure has been done for each row. If two white pixel sequences on consecutive rows are neighboring, they are considered members of the same blob and a same label is assigned to them. Only blob candidates composed by more than N_p pixels are considered valid. Once the blobs on the scene have been determined, the 2D coordinates of every blob center are computed. Figure 4.4 shows an example of the algorithm output.

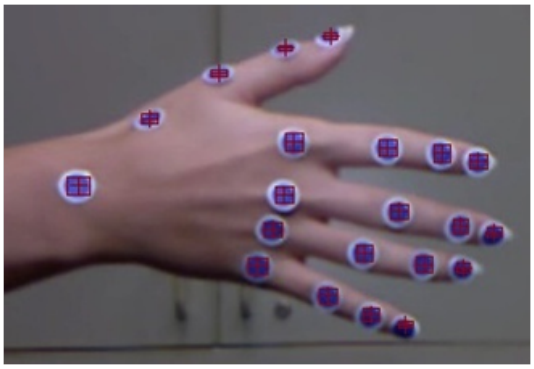

Figure 4.4: Output of blob detection algorithm. The center of each marker is outlined with a red cross.

4.2.3 Tracking

Once the center of each coloured marker has been detected, it is necessary to track the markers during the whole video. Tracking is the process that, assigned a frame at a given time, aims at making coherent correspondences between visible markers on successive frames, while time is passing.

The major problem that the tracking process has to deal with is to make the algorithm robust with respect to the possible appearance/disappearance of markers from the scene and to the presence of outliers due to clutters. A clutter is a condition inside a scene which could induces the blob detection algorithm to identify as marker some noisy blue blobs, that are no actual markers.

As previously said, the pinhole model has been used in order to link the position of scene points with that of their corresponding image points. According to that model, in Fig. 4.5 the position $x_{k,j}$ of the j-th marker, in the k-th frame, on the image plane is shown.

In this thesis a probabilistic approach has been used in order to track and label, in a robust way, the markers attached onto the hand. In the following, the developed algorithm is illustrated in detail.

Let N markers be given, where N is the maximum number of the markers expected in the scene. All the markers projections $j = 1, \ldots, N$ are assumed to

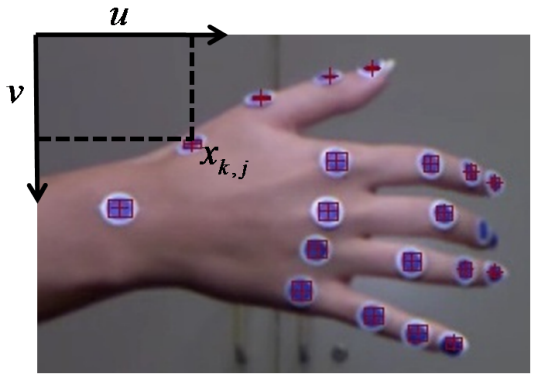

Figure 4.5: Frame k of the video sequence. The coordinate of the j-th marker, $x_{k,j}$, in the reference image plane, are outlined.

have linear state dynamic and measurement models, driven by zero–mean white noises.

Given that $u_{k,j}, v_{k,j}$—the image space coordinates of the j-th marker at the time instant when the k-th frame has been processed—the marker state is defined by

$$x_{k,j} = \begin{bmatrix} u_{k,j} & v_{k,j} \end{bmatrix}^T, \tag{4.2}$$

and thus

$$\begin{cases} x_{k,j} = x_{k-1,j} + w_{k,j} \\ y_{k,j} = x_{k,j} + \nu_{k,j}, \end{cases} \tag{4.3}$$

where

$$w_{k,j} \sim N(0, Q_j) \tag{4.4}$$

$$\nu_{k,j} \sim N(0, R_j) \tag{4.5}$$

The outputs given by the blob detection algorithm, for the k-th image, are given by a random sequence of M_k measurements $\mathbf{Y}_k = \{y_{k,1}, y_{k,2}, \ldots, y_{k,M_k}\}$ of blob candidates. In general the condition $M_k \neq N$ will hold, which means that the sequence $\mathbf{Y}_k$ does contain projections of visible markers and clutters. For example,

the following can be a possible situation:

$$\begin{aligned} y_{k,1} &\rightarrow \text{marker 6} \\ y_{k,2} &\rightarrow \text{marker 7} \\ y_{k,3} &\rightarrow \text{clutter} \\ y_{k,4} &\rightarrow \text{marker 1} \\ y_{k,5} &\rightarrow \text{clutter} \\ y_{k,6} &\rightarrow \text{clutter} \\ &\vdots \\ y_{k,M_k} &\rightarrow \text{marker } h \end{aligned}$$

The randomness of the sequence of measurements is an important issue in this framework, since it implies some important consequences:

- The associations between measurement h and marker j or with a clutter is not a priori decidable and has to be set.
- Each sequence of measurements for each frame can be considered conditionally independent of every other sequence in the past.
- Once the current sequence of associations has been defined, it can be considered conditionally independent of the past history of associations as well.

The last two assumptions state that we consider a certain level of randomness in the blob detection algorithm even in time: this implies that predicting the order in which markers and clutters are detected, for each image, is not allowed.

Because of the above hypotheses, the marker tracking problem actually requires not only the measurement–to-marker association but also a robust marker recognition. The concept of robustness has been dealt with regard to the capability of managing markers appearance-disappearance and of recognizing clutters. Given the intrinsic randomness of the problem, the best way to solve it is by using a general probabilistic approach, via robust Bayesian filtering [83], [84], [85].

The current version of the tracking algorithm does not deal with an explicit hand kinematic model, and thus the markers are treated as mutually independent entities. Measurements are processed one at the time, in a serial fashion, leading to a simplification of the tracking algorithm. Obviously the lack of a kinematic model has to be compensated by some slight complications with respect to the more accurate tuning required for the filter parameters and for the noise matrices of the markers and measurement models. This has been found necessary to avoid swapping situations between markers in some configurations where their projections were very close to each other or overlapping. Even if such hypothesis can be considered conservative enough for the proposed goals, so far the approach has lead to acceptable and accurate tracking results, avoiding the complication of the model. Obviously a more accurate and complex approach can foresee the introduction of a kinematic model of the hand: this would make it possible to constrain the motion of the markers over a sequence of frames.

With the above assumptions, let $a_k \in \{0, 1, 2, \ldots, N\}$ be a discrete indicator variable, defined as follows:

$$a_k = \begin{cases} 0, & \text{if } y_{k,i} \text{ is an outlier;} \\ j, & \text{if } y_{k,i} \text{ is associated to marker } j. \end{cases} \tag{4.6}$$

According to the introduced definition (4.6), the markers model can be converted into a new stacked model. By introducing the augmented markers vector

$$\mathbf{x}_k = \begin{bmatrix} x_{k,1}^T & x_{k,2}^T & \ldots & x_{k,N}^T \end{bmatrix}^T \tag{4.7}$$

and expliciting the definition of the variable a_k, the following Conditional Dynamic Linear Model (CDLM) can be defined:

$$\begin{cases} \mathbf{x}_k = F\left(a_k = j\right)\mathbf{x}_{k-1} + E\left(a_k = j\right)\mathbf{w}_k \\ y_{k,j} = H\left(a_k = j\right)\mathbf{x}_k + \nu_{k,j}, \end{cases} \tag{4.8}$$

where $F\left(a_k = j\right)$ and $E\left(a_k = j\right)$ are selection matrices (they have 1 in the entry

(j, j) and 0 elsewhere), $H(a_k = j)$ is a selection vector (a unit-norm vector e_j^T with 1 in the j–th entry and 0 in the remaining ones).

By conditioning the system on a_k the CDLM (4.8) becomes a linear Gaussian dynamic model. Thus, the state of the j–th marker can be updated once the measure corresponding to that marker has been selected. As already states, since the measure–to–marker association is not a priori known, it is convenient to work with the whole set of markers.

In this work, a "per–measurement" association is used. In the framework of optimal Bayesian filtering, the tracking problem can be defined by estimating the filtering (posterior) distribution

$$p(\mathbf{x}_k|y_{1:k}) = p(x_{k,1}, ..., x_{k,N}|y_{1:k}) \tag{4.9}$$

that is the estimation of the current augmented marker state, given the measurement history up to the current time. With the introduction of the latent variable a_k, the posterior probability $p(\mathbf{x}_k|y_{1:k})$ can be evaluated by marginalization (with respect to a_k) of the joint probability $p(\mathbf{x}_k, a_k|y_{1:k})$, that is:

$$\begin{aligned} p(\mathbf{x}_k|y_{1:k}) &= \sum_{a_k} p(\mathbf{x}_k, a_k|y_{1:k}) \\ &= \sum_{a_k} p(\mathbf{x}_k|a_k, y_{1:k})\ p(a_k|y_{1:k}) \end{aligned} \tag{4.10}$$

The first equality in Eq. (4.10) is obtained by applying the definition of marginalization; the second equality is obtained via Bayes' rule on the joint posterior probability $p(\mathbf{x}_k, a_k|y_{1:k})$.

In the last equality of the Eq. (4.10) two terms are highlighted:

- $p(a_k|y_{1:k})$ is the posterior distribution of the data association, whose shape is, in general, not a priori known, depending on the detection algorithm. Thus a weighted m–samples approximation has to be determined by using Monte Carlo Sequential Importance Resampling (SIR) techniques. In this

work it has been found convenient to use particle filtering as SIR approximation, making it possible to represent the association posterior with a set of particles which are updated and reweighted recursively.

- $p(\mathbf{x}_k|a_k, y_{1:k})$ is the posterior (updated) distribution of the markers projections, conditioned on the association a_k. Given the definition of the CDLM (4.8), it is known that such model becomes a linear Gaussian dynamic model, once the data association is fixed: thus the posterior $p(\mathbf{x}_k|a_k, y_{1:k})$ is actually solved using a Kalman Filter.

From the above analysis, the following relationships hold:

$$p(a_k|y_{1:k}) \approx \sum_{i=1}^{m} w_k^i \delta\left(a_k^i\right) \tag{4.11}$$

$$p(\mathbf{x}_k|a_k, y_{1:k}) = N\left(\hat{\mathbf{x}}_k(a_k),\, P_k(a_k)\right). \tag{4.12}$$

Thus, in view of Equation (4.10) and by using the properties of the Dirac function, the posterior $p(\mathbf{x}_k|y_{1:k})$ is a mixture of Kalman filters, that is:

$$p(\mathbf{x}_k|y_{1:k}) \approx \sum_{i=1}^{m} w_k^i\, N\left(\hat{\mathbf{x}}_k\left(a_k^i\right),\, P_k\left(a_k^i\right)\right) \tag{4.13}$$

where $\hat{\mathbf{x}}_k(a_k^i)$ and $P_k(a_k^i)$ are respectively the mean vector and the error covariance matrix of the Kalman filter associated with the i–th sample (which infers the association a_k^i). The notation $N(\cdot,\cdot)$ indicates the multivariate normal distribution of order 2 which, in general, is given by

$$N(\mu, \Sigma) = \frac{1}{2\pi|\Sigma|^{\frac{1}{2}}} \exp\left\{-\frac{1}{2}(x-\mu)^T \Sigma^{-1}(x-\mu)\right\}. \tag{4.14}$$

According to Eq. (4.13), a set of m particles can be defined, which contains the augmented state mean $\hat{\mathbf{x}}_k$, the error covariance matrix $P_{\hat{\mathbf{x}}_k}$ and the weight w_k^i

associated with each particle, that is

$$\mathcal{S}_k = \left\{ \left(\left\{ \hat{\mathbf{x}}_k^1,\ P_k^1 \right\}, w_k^1 \right),\ \left(\left\{ \hat{\mathbf{x}}_k^2,\ P_k^2 \right\}, w_k^2 \right), \ldots, \left(\left\{ \hat{\mathbf{x}}_k^m,\ P_k^m \right\}, w_k^m \right) \right\} \tag{4.15}$$

Equation (4.10) together with Eq. (4.13) give a direct information about how to solve the filtering distribution $p(\mathbf{x}_k|y_{1:k})$: by generating all the possible hypotheses $a_k = i,\ i = 0, \ldots, N$ and evaluating each of them together with the current observation (by running a Kalman filter), it is possible to evaluate the most likely hypothesis a_k^* which gives the highest score.
By using Bayes' rule, the posterior $p(a_k|y_{1:k})$ can be decomposed as follows:

$$p(a_k|y_{1:k}) \propto p(y_k|a_k, y_{1:k-1})\ p(a_k) \tag{4.16}$$

where $p(y_k|a_k, y_{1:k-1})$ is the likelihood of the measurements and $p(a_k)$ is the association prior, which is assumed to be independent of the previous measurements. The latter is determined by the a priori knowledge of clutter and marker association event probabilities. One way to determine such probabilities is to infer an a priori probability of the clutter event, $p(a_k = 0)$, and to equally split the complementary probability $1 - p(a_k = 0)$ among the N markers association events, that is

$$p(a_k = j) = \frac{1 - p(a_k = 0)}{N},\ j = 1, \ldots, N.$$

This choice is justified by the fact that the probability of detecting the marker j can be assumed to be the same as that of detecting the marker $h \neq j$. In this work this choice has been found to be a valid assumption.

The first possible event is the current measurement to be associated to a marker, say marker j. In this case, the measurement likelihood, given the association $a_k = j$, can be computed, for each particle $i = 1, \ldots, m$, via marginalization

of the joint distribution $p\left(y_k, \mathbf{x}_k\left(j\right)|a_k = j, y_{1:k-1}\right)$:

$$\begin{aligned} p\left(y_k|a_k = j, y_{1:k-1}\right) &= \int p\left(y_k|a_k = j, \mathbf{x}_k\left(j\right), y_{1:k-1}\right) p\left(\mathbf{x}_k\left(j\right)|y_{1:k-1}\right) d\mathbf{x}_k\left(j\right) \\ &= \int p\left(y_k|a_k = j, \mathbf{x}_k\left(j\right)\right) p\left(\mathbf{x}_k\left(j\right)|y_{k-1}\right) d\mathbf{x}_k\left(j\right). \end{aligned} \tag{4.17}$$

The last equality in Eq. (4.17) is justified by the fact that the current measurement is independent of its past history and by recalling the Markovian nature of the marker model.

In the previous equations we have used the notation $\mathbf{x}_k\left(j\right)$ to highlight that we have activated the entries j in the matrices F, E, H.

The prior $p\left(\mathbf{x}_k\left(j\right)|y_{k-1}\right)$ is actually given by a Kalman prediction step, that is:

$$p\left(\mathbf{x}_k\left(j\right)|y_{k-1}\right) = \int p\left(\mathbf{x}_k\left(j\right)|\mathbf{x}_{k-1}\left(j\right)\right) p\left(\mathbf{x}_{k-1}\left(j\right)|y_{k-1}\right) d\mathbf{x}_{k-1}\left(j\right) \sim N\left(\hat{\mathbf{x}}_k^{i-},\, P_k^{i-}\right) \tag{4.18}$$

where

$$\hat{\mathbf{x}}_k^{i-} = F\left(a_k = j\right)\hat{\mathbf{x}}_{k-1}^{i+} \tag{4.19}$$

$$P_k^{i-} = F\left(a_k = j\right)P_{k-1}^{i+}F\left(a_k = j\right)^T + E\left(a_k = j\right)QE\left(a_k = j\right)^T \tag{4.20}$$

being $\mathbf{x}_k^{i-}$ the prediction of the marker positions, obtained via propagation of the last corrected estimation $\mathbf{x}_k^{i+}$, through the marker model. $\mathbf{x}_k^{i+}$ is obtained by using the optimally–associated measurements, collected at the time step corresponding to the previous frame.

On the other hand, $p\left(y_k|a_k = j, \mathbf{x}_k\left(j\right)\right)$ is the probability density function of the measurement y_k, assuming that it has been generated by the j-th marker, which is a linear function of the state, via $H\left(a_k^i = j\right)$ matrix, with Gaussian error, that is

$$p\left(y_k|a_k = j, \mathbf{x}_k\right) = N\left(H\left(a_k^i = j\right)\mathbf{x}_k, R_j\right). \tag{4.21}$$

Thus, by evaluating the integral in (4.17), we have

$$p\left(y_k|a_k=j,y_{1:k-1}\right)=\int N\left(H\left(a_k^i=j\right)\mathbf{x}_k,R_j\right)N\left(\hat{\mathbf{x}}_k^{i-},\,P_k^{i-}\right)d\mathbf{x}_k\left(j\right) \tag{4.22}$$

which allows an analytical computation of the expression of the measurement likelihood function, given the association

$$p\left(y_k|a_k=j,y_{1:k-1}\right)=\frac{1}{2\pi|S_k^i|^{\frac{1}{2}}}\exp\left\{-\frac{1}{2}\left(y_k-\hat{y}_k\right)^T\left(S_k^i\right)^{-1}\left(y_k-\hat{y}_k\right)\right\} \tag{4.23}$$

where

$$\hat{y}_k^i=H\left(a_k^i=j\right)\hat{\mathbf{x}}_k^{i-} \tag{4.24}$$

$$S_k^i=H\left(a_k^i=j\right)P_{k-1}^{i+}H\left(a_k^i=j\right)^T+R_j \tag{4.25}$$

The remaining possibility is the current measurement to be a clutter. Thus, the measurement likelihood for the clutter association can be computed, as usually done in the literature, by considering the clutter events equally distributed along the measurement area/volume. In this framework the measurement space is the image plane, and thus it is possible to write

$$p\left(y_k|a_k=0\right)=\frac{1}{RES_u\times RES_v}, \tag{4.26}$$

where RES_u, RES_v are the numbers of pixels in the u, v direction (image resolution).

Once the expressions of the association prior and of the measurement likelihood have been derived, the importance sampling (i.e. the sampling made on the basis of the normalized probabilities which approximate the importance distribution (1.16)) of the optimal distribution for the association problem can be computed for each particle in the set $\mathcal{S}$. The set of possible associations is discrete, thus the (discrete) value of the association posterior distribution can be computed by inspecting all possible values of the associations, that is:

$$\begin{aligned}\widetilde{p}_0^i &= p\left(y_k|a_k^i=0\right)p\left(a_k^i=0\right)\\ &= \frac{1}{RES_u \times RES_v}p\left(a_k=0\right) \qquad (4.27)\end{aligned}$$

$$\widetilde{p}_1^i = p\left(y_k|a_k^i=1\right)p\left(a_k^i=1\right) \qquad (4.28)$$

$$\vdots$$

$$\widetilde{p}_N^i = p\left(y_k|a_k^i=N\right)p\left(a_k^i=N\right). \qquad (4.29)$$

The final clutter and marker association probabilities are

$$p_0^i = \frac{\widetilde{p}_0^i}{\sum_{h=0}^N \widetilde{p}_h^i} \qquad (4.30)$$

$$p_1^i = \frac{\widetilde{p}_1^i}{\sum_{h=0}^N \widetilde{p}_h^i} \qquad (4.31)$$

$$\vdots \qquad (4.32)$$

$$p_N^i = \frac{\widetilde{p}_N^i}{\sum_{h=0}^N \widetilde{p}_h^i}. \qquad (4.33)$$

Once the sequence p_j^i is defined, it can be used to sample from the optimal distribution $p\left(a_k|y_{1:k}\right)$ and, actually, to implement the tracking algorithm, in order to find the approximation of the posterior

$$p\left(\mathbf{x}_k|y_{1:k}\right) \approx \sum_{i=1}^m w_k^i N\left(\hat{\mathbf{x}}_k\left(a_k^i\right), P_k\left(a_k^i\right)\right)$$

. The algorithm is explained in Tab. 4.1.

Figure 4.6 shows a sequence of hand movements where the blue markers on the hand have to be tracked. At the beginning, there are 25 markers in the scene (Frame 1), at Frame 21 the marker on the MCP joint of the middle finger and the markers on the TIP and DIP joints of the index finger disappear; at Frame 50

the marker on the middle finger MCP joint reappears, but markers on DIP and TIP joint of the index finger are still not present and markers on PIP, DIP and TIP joints of the middle finger have disappeared. In the Frame 55 all the markers reappear. Those results prove the capacity of the algorithm to track the markers in spite of the disappearing marker problem.

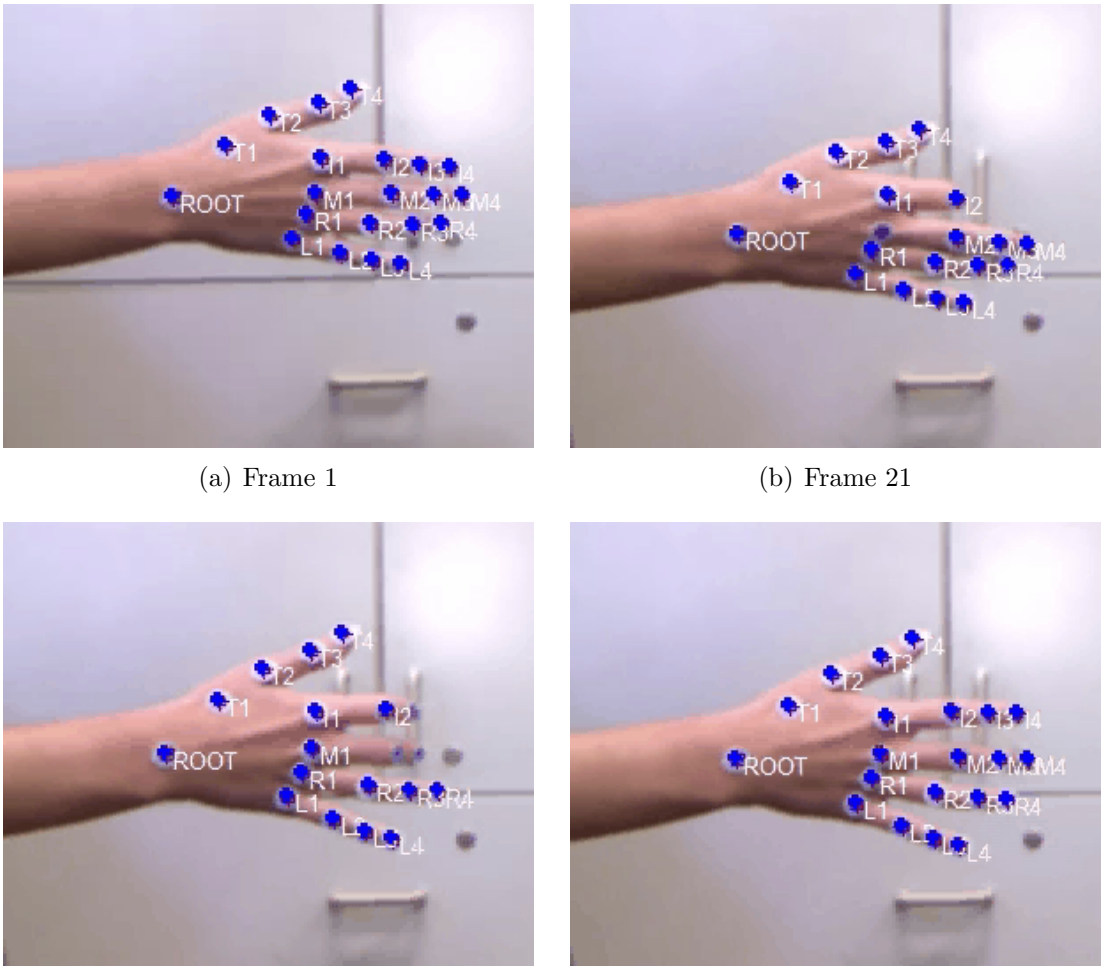

(a) Frame 1

(b) Frame 21

(c) Frame 50

(d) Frame 55

Figure 4.6: Results of the proposed filter based tracking.

With the Kinect motion sensing device it has been possible to perform exper-

iments regarding the movements of the hand, but not about the grasping action. This is due to the fact that, as we have realized, with a single Kinect camera it is possible to obtain information related to simple hand movements. Moreover, the fact that a marker may disappear when the finger is flexed would bring to work with just an estimation of the real joint position. In order to have a broader view of the scene, at least two cameras are needed, but at the moment it is not assured that two Kinect cameras can work facing each other, due to the possible IR interference.

However, the work developed in this thesis can find an interesting application in the rehabilitation field. Usually, a therapist manipulates the injured limb or helps the patient to perform some predefined movements. The repetitiveness of the action is fundamental for helping the patient to re-learn the movements. The idea is to track, using the Kinect camera, the hand movements performed by a therapist, giving the finger trajectories as input to a robotic device attached to the patient hand. The robotic device may subsequently help the patient to perform the movements already done by the therapist. On the basis of the patient residual mobility the therapist chooses the rehabilitation mode according to which the robot should help the patient. If the patient impairment is severe (i.e. the patient cannot move the hand fingers by himself/herself) the robot should move the patient hand in order to follow the pre-registered therapist hand trajectories. When the patient is able to start the movement but is not able to complete it, the robot could operate in the assistive mode, leading the hand to follow the predefined trajectories. The patient motor improvements could be monitored by another Kinect camera, superimposing the therapist finger trajectories with the patient finger trajectories. On the basis of the error, the robotic device could adjust its therapy by resorting to the potentiality of impedance control.

Table 4.1: Tracking algorithm pseudo-code

INIT

- Marker state vector initialization: $\mathbf{x}_0 = \begin{bmatrix} x_{0,1} & ... & x_{0,N} \end{bmatrix}^T$
- Particles initialization: $\mathcal{S}_0 = \{(\{\mathbf{x}_0^1, P_0^1\}, w_0^1), ..., (\{\mathbf{x}_0^m, P_0^m\}, w_0^m))\}$

CICLE

- For each measure $(n = 1 : M_k)$:
  - For each particle $(i = 1 : m)$:
    - ∗ **MKF prediction:** For each hypothesis a_k, run a Kalman prediction step on the couple $\{x_k^i(a_k), P_k^i(a_k)\}$
    - ∗ Calculate the likelihood of the current measure with respect to predictions and to possible associations:
      $$\begin{cases} p_0^i = p(y_k^n | a_k = 0, \mathbf{x}_k^i, \mathbf{y}_{1:k-1}) p(a_k = 0) \\ p_1^i = p(y_k^n | a_k = 1, \mathbf{x}_k^i, \mathbf{y}_{1:k-1}) p(a_k = 1) \\ \vdots \\ p_N^i = p(y_k^n | a_k = N, \mathbf{x}_k^i, \mathbf{y}_{1:k-1}) p(a_k = N) \end{cases}$$
    - ∗ Sample a new association hypothesis a_k^i (particle) from the importance distribution $p\left(a_k | y_k^n\right)$:
      draw $a_k^i = 0$ with normalized probability p_0^i
      draw $a_k^i = 1$ with normalized probability p_1^i
      $\vdots$
      draw $a_k^i = N$ with normalized probability p_N^i
    - ∗ **MKF update:** if $a_k^i \neq 0$, run a Kalman correction step, using the new sampled association variable a_k^i: $\{x_k^i(a_k^i), P_k^i(a_k^i)\}$;
    - ∗ compute the new particle weight: $w_k^i = w_{k-1}^i \sum_h p_h^i$;
  - End for each particle
  - Resample, if necessary, the particle set;
  - Extract the couple $\{x_k^i, P_k^i\}$ from particles with highest probability.
- End for each measure.

Chapter 5

Bio-inspired power-grip posture prediction algorithm

In the previous chapters, the natural mechanisms lying behind the pre-shaping and grasping actions of a human hand have been investigated, in order to adapt them for a robotic hand. Drawing inspiration from neurophysiologic studies on the synergies in the human grasping action, the ultimate purpose of this research is to find a general rule for performing a stable, human-like grasp with a robotic hand.

The study in [86] suggests that the control of hand postures involves a few postural synergies. By combining those primitives it is possible to generate the entire repertoire of movements performed by human beings. In [86], two fundamental synergies for controlling the hand shapes have been identified. The number of synergies increases if more information about the object to be grasped is required. It has also been demonstrated that, during grasping, joint angles of the hand do not vary independently [87]. Hence, the number of active DOFs strictly necessary for controlling the hand shape is smaller than the total number of DOFs of the hand. This entails the feasibility of retrieving general rules for finding grasp configuration algorithms with reduced computational costs.

The main expected benefit of the approach proposed in this thesis is to reduce

the dimension of the space of feasible grasp configurations [88] in order to simplify the complexity of the algorithm, thus avoiding loss of grasp efficiency. It is assumed that two of the three factors that mainly affect the grasping action [27] are pre-defined, i.e. the object physical characteristics and the task to be performed. In particular, object physical characteristics (like shape and weight) affect the hand posture [86] since the pre-shaping phase [28]. Later, when the reaching phase starts, hand aperture increases. It gradually decreases while approaching the object to be grasped in order to mould the hand shape around the object [26].

In this thesis, the attention is focused on cylindrical objects. In [39], for the cylindrical power grasps introduced in the chapters above (transverse volar grasp and diagonal volar grasp), a hand configuration is predicted by modelling the fingers and the object surface with ellipsoids and by applying an optimization algorithm for determining the contact points between the two ellipsoids. The principal drawback of this approach is that the MCP joint adduction/abduction angle is assumed equal to zero and also the thumb adduction/abduction angles need to be estimated. The thumb behavior lacks also in [89] where a criterium for determining the long fingers' optimal grasp configuration for grasping cylindrical object with a diagonal volar grasp is introduced.

The grasping algorithm illustrated in this chapter has the purpose of predicting the optimal hand configuration for firmly grasping a cylindrical object, given the size of the object and its location in the space, filling up the deficiencies of the approaches previously exposed. It resorts to (i) published results of biomechanics in [89] regarding the optimal configuration of the long fingers of the human hand during a diagonal volar grasp and (ii) our results on human motion analysis, presented in Chapter 3, to extend the approach to the five fingers (including thumb) and to the transverse volar grasp.

Once the hand configuration for an optimal grasp has been defined, it is necessary to establish the trajectory that the fingers should follow in order to get the final grasp configuration. In order to overcome this problem, over the years the mechanical structure of robotic hands has been considered along with algo-

rithms for improving grasping naturalness. For instance, in [90] under-actuated prosthetic hands that try to reproduce the gradual moulding of the hand on the object contour by automatically adapting themselves to the object shape are introduced. In [91] the minimum jerk approach is fitted to a prosthetic finger. The main drawback is that the approach is suited only for straight movements in the xy-plane, while the fingers trajectory of the human hand is curved. Two optimization-based models are proposed in [92]. In the former approach, the function to be minimized is analogous to the kinetic energy. It implies constant velocity and acceleration values, which is against the bio-inspired assumptions of null start and final joint velocity valid for finger movements. The latter approach, based on minimum torque-change cost function, has the drawback that the curvature of the finger path is opposite to that observed in experiments on human beings. In a prosthetic hand driven by electromyographic signals (EMG), for example, once the command given by the patient has been interpreted, the prosthetic hand has to move autonomously following a suitable trajectory. In this thesis, taking inspiration from [93], the fingertip movement is modelled with a logarithmic spiral.

5.1 Human-like grasping algorithm

5.1.1 Optimization algorithm

The wrist plays a fundamental role in the grasping action, i.e. it guides the hand to the grasp position and adjusts the orientation on the basis of the grasping type and task. This is the reason why one marker has been positioned on the wrist of the examined human subjects during the motion analysis with the Vicon and the Kinect systems and why, in the bio-inspired grasping algorithm illustrated in the following, a point on the wrist, called CarpoMetaCarpal (CMC) joint, is considered as reference point for determining the position of the other hand joints.

In [89] it has been shown that the optimal configuration of the long fingers, for

grasping a cylindrical object with a diagonal volar grasp, is the one that minimizes the sum of the distances between the hand joints and the object surface. In this thesis, this approach has been first applied to four fingers of a robotic hand in order to test the reliability of the findings [94]. Moreover, the experimental results in Tab. 3.5 show that long fingers configurations in a diagonal volar grasp and in a transverse volar grasp are very similar, thus supporting the extension of the optimization algorithm to the transverse volar grasp.

Therefore, the optimization algorithm for predicting the long finger configuration both in a diagonal volar grasp and in a transverse volar grasp, can be formulated as follows. The position of the CMC joint that guarantees a stable grasp configuration can be obtained by minimizing the objective function given by the sum of the distances of all finger joints from the object surface. It can be written as

$$f = \sum_{i=1}^{4} \sum_{j=1}^{3} dist_j^i(z, \alpha), \tag{5.1}$$

where

- j is the joint index, ranging from 1 (the MCP joint) to 3 (the DIP joint);
- $dist_j^i(z, \alpha)$ is the distance of the j-th joint of the i-th finger from the object surface (red dotted line in Fig. 5.2). This distance is a function of z, i.e. the CMC z-coordinate in the reference frame of Fig. 5.2, and of α, i.e. the inclination angle of the hand reference frame y-axis with respect to the object rotation axis (see Fig. 5.1);
- r_{obj} is the object radius.

A schematic representation of the finger interacting with the object is shown in Fig. 5.2. It is assumed that the object physical characteristics, i.e. position and shape, are a priori known. A reference frame centred in the hand CMC joint is defined (Fig. 5.2). The positions of the object and of all the hand joints (MCP,

PIP and DIP) are computed with respect to this coordinate system. The palm of the tight hand faces the object, and the fingers are parallel to the z-axis of the reference frame.

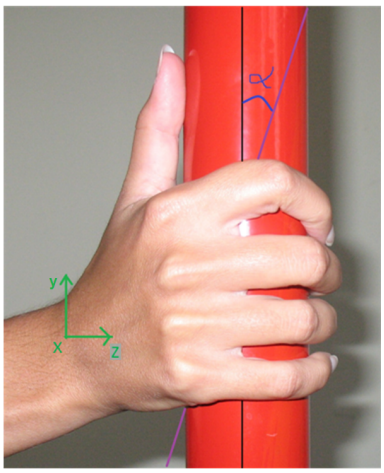

Figure 5.1: Human grasp of a cylindrical object. The black line is the object rotation axis, the blue line is the y-axis of the object in case the hand is inclined of a certain angle α. The reference frame is outlined in green.

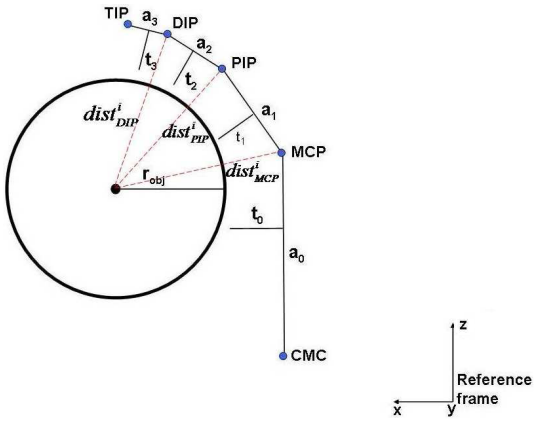

Figure 5.2: Schematic representation of the virtual scenario in which the algorithm has been developed.

As evident from Fig. 5.1, during a volar grasp, the fingers of a human hand are

not parallel, but are inclined of certain angles. However, for the sake of clarity, a simpler case is first considered, in which the fingers are parallel to each other. Later, the extension to the case of inclined fingers is explained.

In the case of parallel fingers, the planes where the fingers lie are perpendicular to the object rotation axis (the black line in Fig. 5.1). For each joint (i.e. MCP, PIP and DIP), the distances from the object surface can be expressed as

$$dist^i_{MCP} = \sqrt{(z_{MCP_i} - z_{obj})^2 + (r_{obj} + t_0)^2} \tag{5.2}$$

$$dist^i_{PIP} = \sqrt{(a_1 - \sqrt{(r_{obj} + dist^i_{MCP})^2 - (r_{obj} + t_1)^2})^2 + (r_{obj} + t_1)^2} \tag{5.3}$$

$$dist^i_{DIP} = \sqrt{(a_2 - \sqrt{(r_{obj} + dist^i_{PIP})^2 - (r_{obj} + t_2)^2})^2 + (r_{obj} + t_2)^2} \tag{5.4}$$

where

- a_i is the finger length,
- t_i is the finger thickness,
- z_{MCP_i} is the z-coordinate of the MCP joint of the i-th finger in the optimal configuration. Its value depends on the z-coordinate of the initial configuration (i.e. $z^{start}_{MCP_i}$) and on the inclination angle α given by the optimization procedure. In particular, z_{MCP_i} can be expressed as

  $$z_{MCP_i} = z + (z^{start}_{MCP_i} - z^{start}_{MCP_4}) + (y^{start}_{MCP_i} - y^{start}_{MCP_4}) * tan\alpha \tag{5.5}$$

  where it has been supposed that, in the optimal configuration, the z-coordinate of the little finger MCP joint coincides with the object z-coordinate (Fig. 5.3).

Therefore the z-coordinate of the MCP joint of any other finger is computed with respect to that of the little finger.

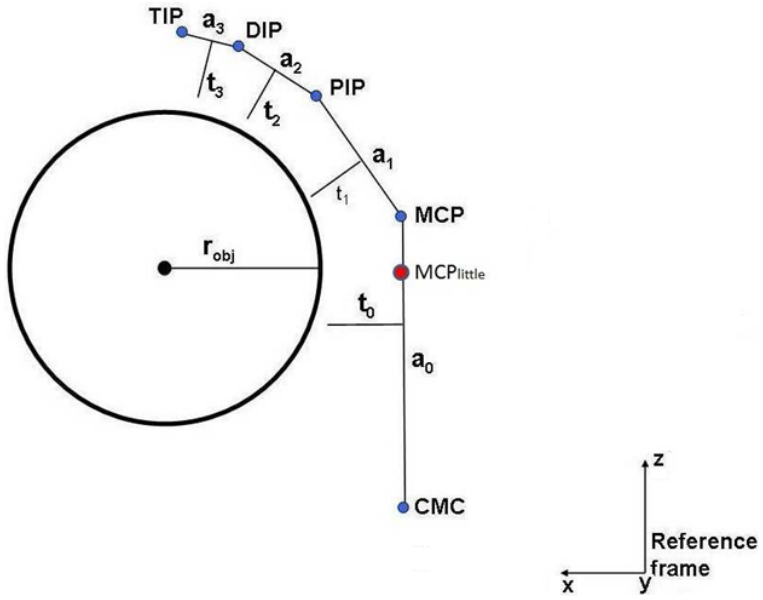

Figure 5.3: Schematic representation of the virtual scenario in which the MCP little position is outilined in red.

When fingers lie on planes inclined with respect to the plane perpendicular to the object rotation axis (plane zx in Fig. 5.2), the joint projections in this plane are considered. These values are determined by replacing the link length a_i in the distance equations (5.2)–(5.4), with the link length projections l_k computed by considering the vector normal to the zx-plane of Fig. 5.2. In Fig. 5.4 some of the link projections on the zx-plane are shown. The red dot is the CMC joint, the green dots are MCP, PIP and DIP joints of the index finger, the blue dots are MCP, PIP and DIP joints of the middle finger, the magenta dots are MCP, PIP and DIP joints of the ring finger and the black dots are the MCP, PIP and DIP joints of the little finger. Finger thickness should be considered, because the represented points are the finger joints.

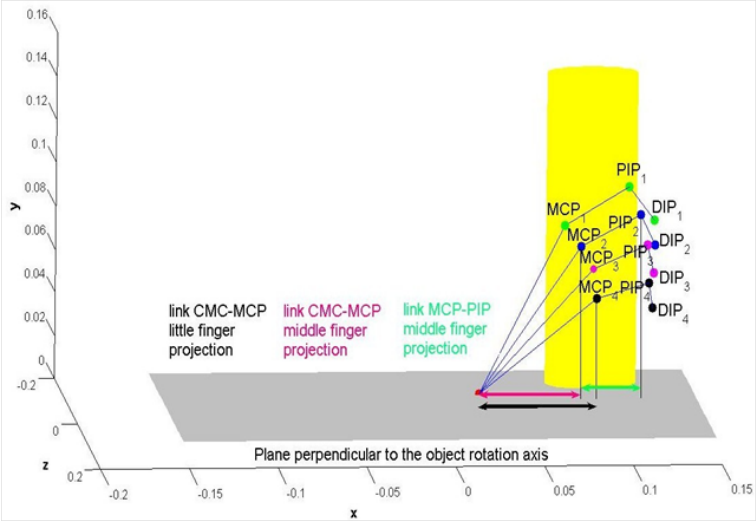

Figure 5.4: Plot of the hand during grasping of a cylindrical object in the case of inclined finger. Some of the link projections on the zx-plane are outlined with different colours.

The link length projection value l_k is determined in the projection plane using the following expression:

$$l_k = a_k^2 - \| a_k \bullet (n_p \times n_o) \|^2 + (n_p \bullet n_o)^2 + \| a_k \bullet (n_p \times n_o) \|^2 \qquad (5.6)$$

where $n_p \times n_o$ and $n_p \bullet n_o$ are respectively the cross product and the dot product between the unit normal vector n_p of the plane perpendicular to the object rotation axis and the unit normal vector n_o of the oblique plane where the fingers lie.

In this way it is possible to work in the projection plane, going back to the simplified case of parallel fingers. Thus, joint Cartesian coordinates determined in the projection plane are brought back to the original planes where the fingers lie trough a rotation matrix, since the inclination angle is known. Joint angles are determined by means of inverse kinematics, starting from the joint Cartesian coordinates.

Hence, through eqs. (5.1) to (5.5), by providing the CMC z-coordinate and the distances of the joints from the object surface, in addition to some geometrical

considerations, all the joint coordinates are computed for the four long fingers in such a way as to have a human-like optimal grasp configuration.

Still relying on studies on human beings [22], [76], a constraint is imposed on the DIP and PIP flexion angles. In particular the following relation is used for coupling the two joints: $\theta_{DIP} = \frac{2}{3}\theta_{PIP}$.

As regards the thumb, an important finding can be retrieved by the experimental data on human subjects in Chapter 3: the hand aperture angle is quite invariant from subject to subject when a transverse volar grasp is performed (see Tabs. 3.4 and 3.6). Therefore, assuming that the aperture angle is known, the MCP joint position with respect to the CMC joint can be found, thus enabling the extension of the optimization algorithm also to the thumb. This means that the position of the other thumb joints can be obtained by minimizing the distances from the thumb joints and the object surface by means of 5.2– 5.5.

5.1.2 Trajectory planning algorithm

Once the optimal hand joint positions have been determined, it is necessary to move the fingers from the initial configuration to the final one given by the preshaping optimization algorithm, by following a reference trajectory.

On the basis of studies on the human beings [93] it is possible to say that the fingertip motion during grasping follows a logarithmic spiral trajectory. In the Cartesian space, the time-varying coordinates of the TIPs are:

$$\begin{cases} x = r\cos\theta \\ y = r\sin\theta, \end{cases} \tag{5.7}$$

They corresponds to a logarithmic spiral in polar coordinates

$$r = ae^{b\theta} \tag{5.8}$$

where r is the spiral radius, a is a coefficient that rotates the spiral, b is a coefficient that controls spiral pitch and twins direction, and θ is the angle between

the radius and the z-axis of the reference frame centred in the MCP joint. It is evident that the radius of the spiral depends on the spiral inclination angle θ that fingers sweep.

Equations (5.7)– (5.8) allow determining the points the fingertips will pass through when moving from an initial position (full open hand near the object) to the final position of the joints computed by the minimization algorithm (Fig. 5.5).

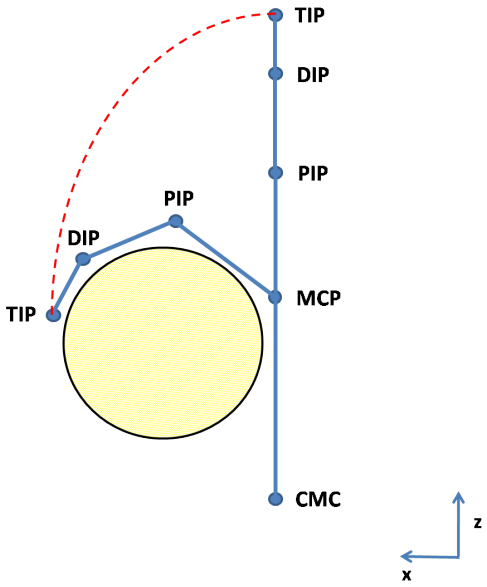

Figure 5.5: Finger position at the beginning and at the end of the trajectory.

The joint angles corresponding to the TIP positions during grasping are obtained using the inverse kinematics. A proportional-derivative control in the joint space is used to make the hand track the reference trajectory in (5.8).

A schematic representation of how the two algorithm work together is shown in Fig. 5.6: starting from information about initial joint angles, the optimization algorithm gives us the joint positions that the hand will have to assume at the end of the grasping action for a stable grasp. The algorithm returns also the CMC optimal position near the object. After the reaching phase, in which the hand reaches the position in which the CMC joint position is the one defined by

the algorithm, initial finger joint angles and optimal finger joint angles are given in input at the trajectory planning algorithm whose output is the path that the fingers will follow for a natural grasping action.

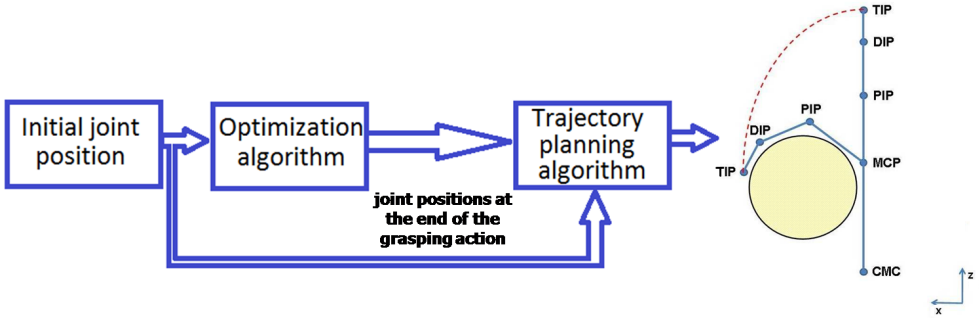

Figure 5.6: Finger position at the beginning and at the end of the trajectory.

5.2 Experimental validation of the grasping algorithm

The ultimate purpose of this thesis is to test the reliability of the grasping algorithm explained above in a real arm-hand robotic system. The grasping action is divided in two parts: in the former, the hand moves towards the object so that the CMC joint is in the optimal position for a stable grasp; in the latter, the hand fits the object shape.

5.2.1 Experimental setup

The experimental platform (Fig. 5.7) on which the algorithm has been validated is composed of the MIT-Manus planar robot, which acts like the arm and realizes the reaching task, and the DLR-HIT-Hand II which is mounted at the MIT-Manus end-effector and is responsible for preshaping and grasping. Two cylindrical objects with two different sizes, chosen compatibly with the mechanical constraints

of the hand (diameter of 0.022.5 m and 0.020 m, respectively), have been selected. Figure 5.7 shows the MIT-Manus reference frame $(x_{manus}, y_{manus}, z_{manus})$, the DLR-HIT-Hand II reference frame $(x_{DLR}, y_{DLR}, z_{DLR})$, the initial hand configuration, given in the MIT-Manus reference frame, and the object to grasp.

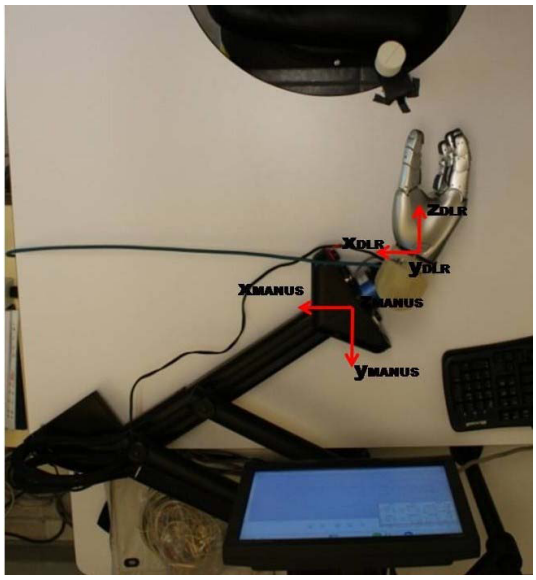

Figure 5.7: Experimental setup. The DLR-HIT-Hand II and MIT Manus reference frames are shown.

The MIT-Manus system (shown in Fig. 5.7) is a planar robotic arm (typically used for upper-limb rehabilitation) with two rotational degrees of freedom, one for the elbow and one for the shoulder angular motion. It reproduces the planar motion of shoulder and elbow rotational joints of the upper limb in a workspace of 0.40x0.40 m. It is equipped with two optical absolute encoders and a six-axis JR3 force/torque sensor. The Denavit-Hartenberg parameter are shown in Tab. 5.1.

The five-fingered dexterous robotic hand DLR-HIT-Hand II (Fig. 5.8) has an independent palm and five identical modular fingers. Each finger has four DOFs (adduction/abduction of the MCP joint, flexion/extension of the MCP, PIP and DIP joints), three of which are actuated and one is passive. The last two joints (PIP and DIP) are 1 : 1 coupled, meaning that the corresponding

Table 5.1: MIT-Manus Denavit-Hartenberg parameters.

Link #	d	θ	$a\,[m]$	α
0	0	0	0	0
1	0	0	0.551	$-\frac{\pi}{2}$
2	0	0	0.407	$-\frac{\pi}{2}$

flexion/extension angles are equal. The thumb is mechanically constrained to assume a fixed opposition of 35.51^o in the xy-plane with an inclination, with respect to z-axis, of 44.13^o; this enables only transverse volar grasps with a fixed thumb inclination.

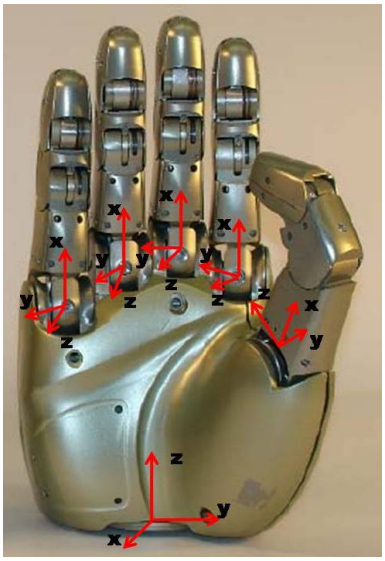

Figure 5.8: DLR-HIT Hand II with hand and finger reference frames.

All the active DOFs of the hand are actuated by flat brushless DC motors. Actuators and electronic circuits are embedded in fingers and palm mechanical structure. Furthermore, each finger has three Hall-effect sensors for measuring joint positions, two force/torque sensors and one thermistor as temperature sensor.

Hand geometric data and Denavit-Hartenberg parameters are listed in Tabs. 5.2 and 5.3, respectively.

Table 5.2: DLR-HIT-Hand II geometric parameters.

Symbol #	Link name	value$[m]$
a_{01}	$CMC - MCP_{index}$ link length	$117x10^{-3}$
a_{02}	$CMC - MCP_{middle}$ link length	$118.3x10^{-3}$
a_{03}	$CMC - MCP_{ring}$ link length	$117x10^{-3}$
a_{04}	$CMC - MCP_{little}$ link length	$105x10^{-3}$
a_1	Proximal link length	$55x10^{-3}$
a_2	Medial link length	$25x10^{-3}$
a_3	Distal link length	$25x10^{-3}$
t_0	Palm thickness	$62x10^{-3}$
t_1	Proximal link thickness	$35x10^{-3}$
t_2	Medial link thickness	$26x10^{-3}$
t_3	Distal link thickness	$24x10^{-3}$

Table 5.3: DLR-HIT-Hand II Denavit-Hartenberg parameters.

Link #	$d\,[m]$	θ	$a\,[m]$	α
0	0	0	0	0
1	0	0	0	$-\frac{\pi}{2}$
2	0	0	0.055	0
3	0	$-\frac{\pi}{2}$	0.025	0
4	0.025	π	0	$-\frac{\pi}{2}$

The object to be grasped is a cylinder whose shape, weight and position are known. The initial configuration of the hand joints, as well as the optimal configuration computed by the algorithm, have been provided in the MIT-Manus reference frame. Being the MIT-Manus planar, the arm and hand height from the table could not be varied. Consequently, the object was properly located in order to allow closing the middle finger at half of the object height. This assumption is coherent with studies on human beings [95].

Given the object position, the optimal CMC Cartesian position and the final

hand configuration for grasping the object have been obtained by minimizing (5.1) through the MATLAB function $fminsearch(f, [initialcondition])$. During the reaching movement, the hand has been moved by the arm towards the optimal CMC position. Thus, the hand has been controlled in order to reach the final MCP, PIP, DIP joint angles, also provided by the optimization algorithm. During reaching, the hand cannot change orientation, since the arm motion is planar: z_{DLR}-axis is always parallel to y_{MANUS}.

A fifth-order polynomial function has been used to plan the MIT-Manus linear motion from the initial position up to the final position. Then, a proportional-derivative (PD) torque control in the Cartesian space has been used to control arm position, and consequently CMC position, in the plane.

As regards preshaping, final MCP, PIP and DIP joint positions, provided by the optimization algorithm, have been taken as reference for the DLR-HIT-Hand II motion controller. A third-degree polynomial function has been used to plan the joint motion up to the final reference value and a PD torque control in the joint space has enabled reaching the desired final angles. It is worth noticing that, in the DLR-HIT-Hand II, the DIP and PIP joints are coupled with $\theta_{DIP} = \theta_{PIP}$, thus imposing a constraint on the final position of DIP and TIP, that is often slightly different with respect to the desired one.

5.2.2 Simulation results

The described algorithm has been firstly validated in a simulated environment with the same characteristics of the real one, where the MIT-Manus and DLR-HIT-Hand II kinematics and dynamics were modelled. The obtained results are shown in Figs. 5.9 and 5.10 for a diagonal volar grasp and a transverse volar grasp, respectively.

In order to obtain the thumb position, the results obtained with the Vicon and the CyberGlove motion analysis system have been used. The aperture angle values reported in Chapter 3 let us obtain the position of the thumb MCP joint with respect to the CMC joint. The other joint positions, as previously explained,

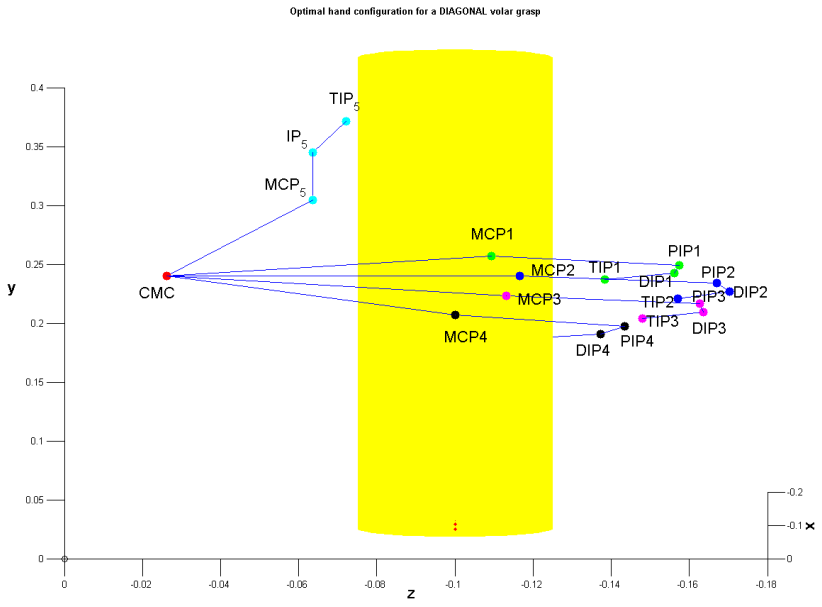

Figure 5.9: Plot of the object and hand joint positions in the optimal DIAGONAL grasp configuration.

are computed by minimizing the distance from the object surface.

5.2.3 Experimental results

The proposed algorithm has been experimentally tested on the MIT-Manus and the DLR-HIT-Hand II. The obtained results are shown in Fig. 5.12, where the joint trajectories are shown in the Cartesian space.

The values obtained from the optimization algorithm (i.e. CMC position and flexion and adduction angles for all fingers) have been given in input to the real arm-hand robotic system. The MIT-Manus moves the hand in such a way that its CMC joint reaches the position defined by the algorithm. Thus, the hand closes the fingers to reach the desired angles for each joint.

For the arm, a point-to-point movement has been performed in 3.0 s for each

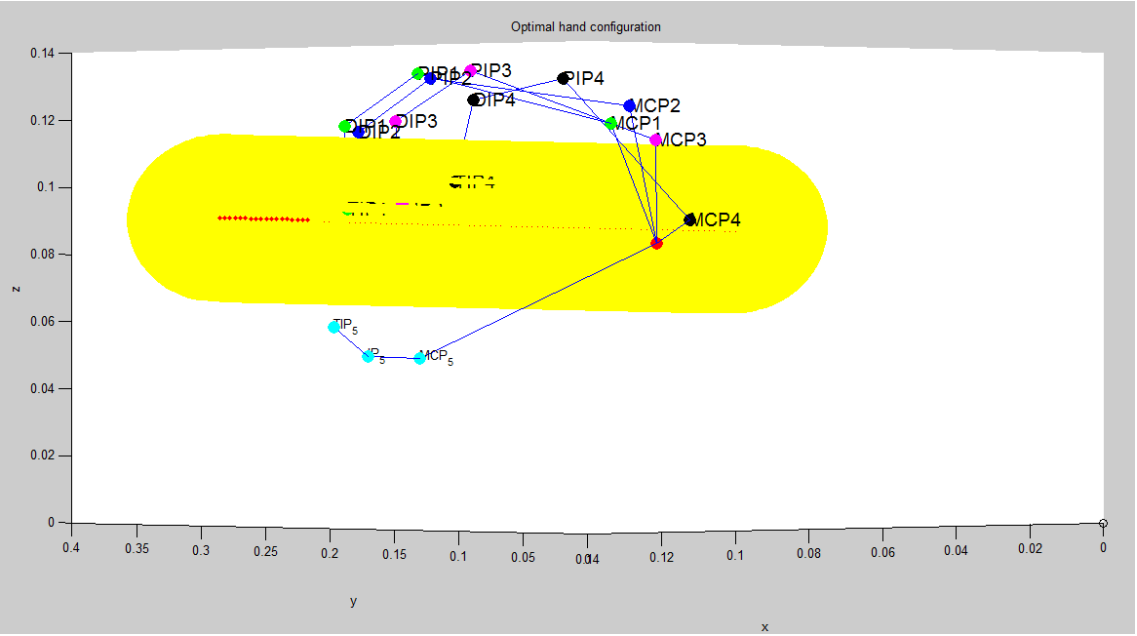

Figure 5.10: Plot of the object and hand joint positions in the optimal TRANSVERSE grasp configuration.

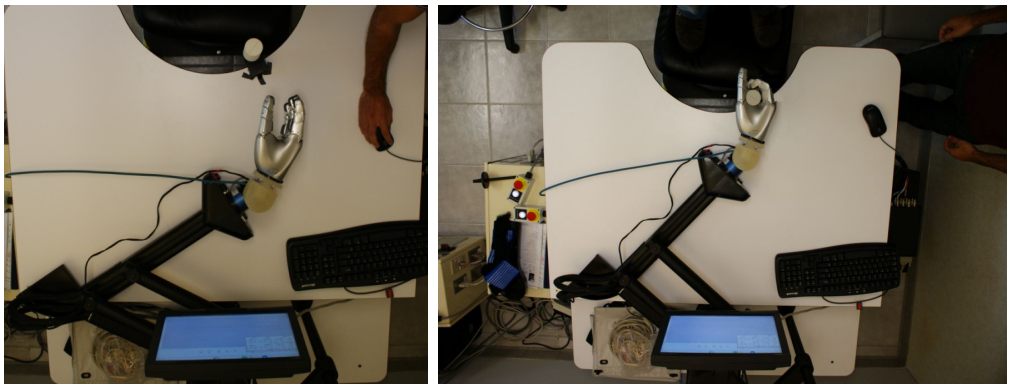

(a) (b)

Figure 5.11: (a) Starting point of the reaching phase; (b) Grasping action completed.

trial, starting from the initial position $P_i = [-0.1 \quad 0.1]^T$ m to the final posi-

tion $P_f = [-0.0975 \quad -0.1245]^T$ m. The final position, reported for the sake of brevity only for the case of grasping an object with radius of 0.020 m, takes into account the CMC position supplied by the algorithm $CMC = [-0.0975 \quad -0.179 \quad 0.15]^T$ m as well as the offset between the arm end-effector and the hand CMC due to the flange that connects the DLR-HIT-Hand II to the MIT-Manus robotic arm. The robotic arm has been controlled for 5.0 s in each trial: (i) three seconds are taken to achieve the final position; (ii) in the last two seconds, the robot holds its posture to enable the grasping phase, lasting 1.2 s. The cylindrical objects to grasp have radii 0.0225 m and 0.020 m and have been located in $(-0.051, -0.257)$ m in the MIT-Manus reference frame. Once the CMC optimal position has been reached, the hand fingers are moved towards the optimal joint configuration (see Fig.5.11).

The control gains used for the MIT-Manus PD control in the Cartesian space and the DLR-HIT-Hand II PD control in the joint space are, respectively:

- K_PA =diag$\{850, 850\}$ N/m and K_DA =diag$\{50, 50\}$ Ns/m
- $K_PM = 0.3$ Nm/rad and $K_DM = 0.02$ Nms/rad for the MCP joint of each finger; $K_PP = 0.4$ Nm/rad and $K_DP = 0.027$ Nms/rad for the PIP joint of each finger.

Actual Cartesian coordinates for each joint of the robotic hand performing the transverse grasp have been computed and compared with the Cartesian coordinates produced by the optimization algorithm. The main observation concerns the difference in the Cartesian coordinates for the algorithm and the robotic hand and, consequently, for the human hand finger joints. Differences are due to the mechanical structure of the robotic hand that constrains the motion of the thumb and the DIP joints in a way that is different with respect to the human hand. In particular, the robotic thumb is mechanically constrained to a fixed opposition of 35.51^o in the xy-plane with an inclination of 44.13^o with respect to z-axis; instead, from the analysis of the data obtained with the Vicon system on the human subjects, the angle in the xy-plane is on average 33^o and the angle with respect

to z-axis is around 37^o. Also the aperture angle is different: about 37^o for the robotic hand, 56^o on average for the human hand. Since the algorithm is based on data obtained from the observation of human behavior, there is obviously a difference in the experimental results, due to the different mechanical structure of the hand performing the task.

Nevertheless, interestingly enough, the values obtained for the radius of curvature of the joints of the DLR-HIT-HAND II are very similar to those computed using the data obtained from the algorithm and from the observation of human beings (see Tab. 5.4). Table 5.4 provides the values of the radius of curvature for the robotic hand in the grasping configuration compared with the values calculated for human case and for the output of the optimization algorithm, for an object radius of 0.0225 m. The radii of curvature have been computed for the three systems as previously exposed in Chapter 3.

Table 5.4: Values of the radius of curvature calculated for the human subject, the output of the optimization algorithm and and the robotic hand, in the case of object radius = 0.0225 m.

		Values of radius of curvature (m)		
Finger	Joint	Human being	Algorithm	Robotic hand
index	MCP	$9.55 * 10^{16}$	$6.96 * 10^{14}$	$3.85 * 10^{14}$
	PIP	0.028	0.024	0.025
	DIP	0.033	0.029	0.019
	TIP	$1.01 * 10^{17}$	$2.36 * 10^{14}$	$4.24 * 10^{14}$
middle	MCP	$7.48 * 10^{16}$	$5.75 * 10^{15}$	$5.9 * 10^{14}$
	PIP	0.037	0.024	0.022
	DIP	0.032	0.028	0.016
	TIP	$8.9 * 10^{16}$	$2.2 * 10^{15}$	$6.5 * 10^{14}$
ring	MCP	$7.16 * 10^{16}$	$7.7 * 10^{15}$	$8.58 * 10^{13}$
	PIP	0.037	0.023	0.24
	DIP	0.038	0.03	0.018
	TIP	$9.94 * 10^{16}$	$1.49 * 10^{15}$	$6.98 * 10^{13}$
little	MCP	$6.58 * 10^{16}$	$9.9 * 10^{13}$	$7.95 * 10^{15}$
	PIP	0.043	0.033	0.027
	DIP	0.032	0.014	0.020
	TIP	$1.14 * 10^{17}$	$1.11 * 10^{14}$	$1.68 * 10^{14}$
thumb	TM	$3.22 * 10^{16}$	$7.01 * 10^{14}$	$2.8 * 10^{14}$
	MCP	0.051	0.018	0.043
	IP	0.028	0.025	0.032
	TIP	$9.66 * 10^{16}$	$8.45 * 10^{13}$	$1.41 * 10^{14}$

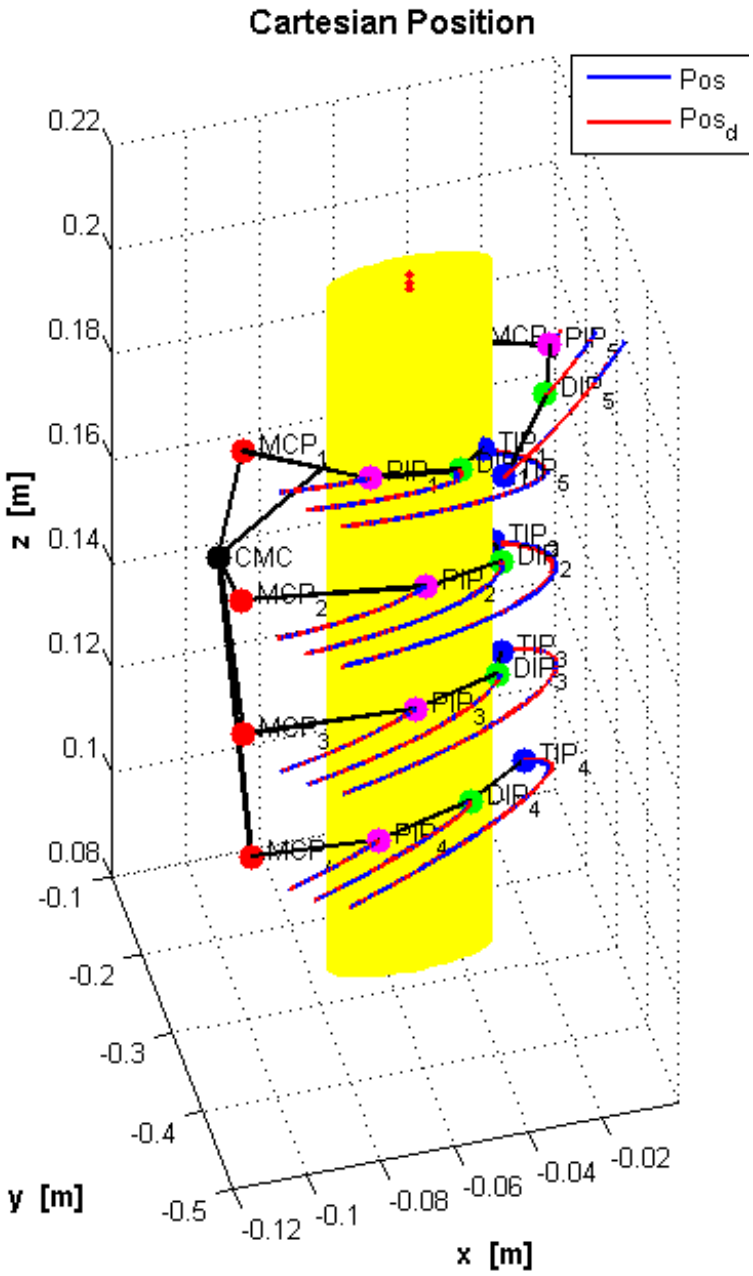

Figure 5.12: Hand joints trajectory in the Cartesian space for the DLR-HIT-Hand II grasping the cylindrical object with radius 0.020 m.

Chapter 6

Epilogue

In this conclusion and future work chapter, a brief review about the thesis aim and the obtained results is presented. Proposals for future researches are also discussed.

6.1 Conclusion

The literature analysis has highlighted the attempt of researchers to create biologically inspired robotic systems. The effort to replicate the human behavior is at the basis of medical robotics, whose aim is substituting or recovering the lost human motor capabilities. Different approaches have been proposed for characterizing grasping in order to improve control and sensing of the robotic hands.

The contribution of our study of the human grasping action has been the identification of some common behaviors among different human subjects. The results obtained with different motion analysis systems have led us to find some general criteria for performing a stable human-like grasp.

A biologically inspired approach for finding the optimal grasp configuration has been also presented. It focuses on the prediction of the final position of the reaching movement and of the optimal finger configuration for a power grasp, once information on object size and location has been provided. The preshaping

phase is the core of our research since ensuring an appropriate finger configuration reduces the complexity of the control that ensures stability of the grasp. The algorithm accounts for data on human subjects partly retrieved from the literature and partly obtained by the direct observation of human behavior during diagonal and transverse volar grasps. The proposed approach, on one hand, provides new insights into the comprehension of the human grasping strategy and, on the other hand, provides a general rule for grasping cylindrical objects with an anthropomorphic robotic hand. The algorithm is focused on the hand kinematics neglecting the dynamics since one of the work aims is to provide some hints for improving the design of the existing robotic hands. Our purpose has also been to give importance at the thumb role during grasping. The robotic hands developed until now do not allow a human-like use of the thumb: some of them have a thumb in a quite fixed configuration; others have a thumb identical to the other fingers and placed in a non-anthropomorphic configuration. The findings on the human thumb behavior enable us to introduce some motor constraints in the grasping algorithms assuring a grasp performed in a human-like manner. Once the optimal hand configuration has been found, the trajectory planner lets the hand grasp the object in the most natural way.

The power-grip posture prediction algorithm has been preliminarily tested in simulation and then validated through experimental trials with a real arm-hand robotic system, composed of the MIT-Manus robot arm and the DLR-HIT-Hand II. Experimental results on the described robotic platform have proved its feasibility and reliability, but have also shown limitations in the grasping capability due to the constraints imposed by the used mechanical structure, not similar enough to the human structure.

To summarize, the human-based approach for determining the optimal grasp configuration returns at first the optimal position of the wrist joint with respect to the object. The algorithm output consists also of the optimal joint angles that ensure a stable grasp. The trajectory planning algorithm moves hand fingers so that the optimal configuration is reached. A schematic representation of the

algorithms is shown in Fig. 6.1.

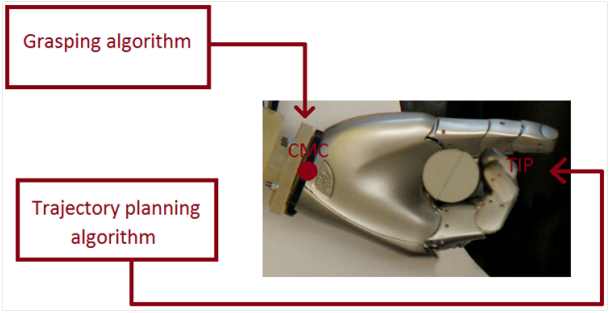

Figure 6.1: Schematic representation of the bio-inspired grasping algorithms.

One more contribution of the thesis has been the realization of the software for using the Kinect motion sensing device for analysing the hand movements. In order to track the hand movements some markers have been placed on the hand joints with a properly configuration. An algorithm based on Bayesian estimation theory and on filtering techniques has been implemented. However, using a single Kinect camera has revealed to be inadequate to obtain reliable information about the grasping action since, when a finger is flexed (i.e., markers disappear), we would work with just an estimation of the real joint position. In order to overcome this problem it could be possible to work with more than one Kinect, so as to have information about the scene from different perspectives. Since Kinect cameras have IR projectors, it could be possible that IR rays interference among each other. Therefore it is necessary to test the possibility to work with two or more Kinect facing each other. However, the data obtained with the Kinect camera could have an application in the rehabilitation field as explained in the following section.

6.2 Future works

For what concerns further analysis of the human grasping action, future works will regard the investigation of the pinch, lateral and tripod grasp data already

acquired during the experiments performed with the Vicon and the CyberGlove.

A future application of the implemented tracking algorithm with the Kinect could be in the field of rehabilitation robotics for creating a new interface for a hand rehabilitation device. The first step would be the observation with the Kinect camera, and the subsequent quantitative description of what the human therapist does. Special attention should be devoted to identify TIP trajectory that will be given in input to a robotic device attached to the patient hand. Afterwards, the robotic device could help the patient to follow the desired trajectories. The patient motor abilities and its progresses will be monitored with the Kinect itself, by superimposing the optimal trajectory, previously performed by the therapist and memorized in the robot arm, with the trajectory executed by the patient.

In order to have a broader view of the scene, we want to ascertain whether two Kinect cameras can work facing each other. If we will get an affirmative answer, the application of the Kinect and of the tracking algorithm could be extended to the grasping action analysis.

Bibliography

[1] G. Schlesinger, "Der mechanische aufbau der kunstlichen glieder," *Ersatzglieder und Arbeitshilfen*, 1919.

[2] M. Cutkosky, "On grasp choice, grasp models and the design of hands for manufacturing tasks," *IEEE Transactions on Robotics and Automation*, 1989.

[3] M. Santello and J. Soechting, "The nature of human prehension three dexterous hand in one," *Proceedings of IEEE International Conference on Robotics and Automation*, pp. 396–401, 1987.

[4] M. Hillman, "Rehabilitation robotics from past to present — a historical perspective," *Advances in Rehabilitation Robotics*, vol. 306, 2004.

[5] H. van der Loos and D. Reinkensmeyer, "Rehabilitation and health care robotics," *Springer Handbook of Robotics*, 2008.

[6] D. Erol, V. Mallapragada, N. Sarkar, and E. Taub, "A new control approach to robot assisted rehabilitation," *9th International Conference on Rehabilitation Robotics*, 2005.

[7] S. Subramanian, L. A. Knaut, C. Beaudoin, J. B. McFadyen, A. G. Fedman, and M. F. Levin, "Virtual reality environments for post-stroke arm rehabilitation," *Journal of Neuroengineering and Rehabilitation*, vol. 4, no. 20, 2007.

[8] P. Lum, D. Reinkensmeyer, R. Mahoney, W. Z. Rymer, and C. Burgar, "Robotic devices for movement therapy after stroke," *Topics in Stroke Rehabilitation*, vol. 8, no. 4, pp. 40–53, 2002.

[9] L. Zollo, M. Passalacqua, D. Formica, and E. Guglielmelli, "Performance analysis of adaptive interaction control laws for rehabilitation robotics," *Proceedings of the IEEE/RAS-EMBS International Conference on Biomedical Robotics and Biomechatronics*, 2008.

[10] M. W. O'Dell, C. Lin, and V. Harrison, "Stroke rehabilitation–strategies to enhance motor recovery," *Annual Review of Medicine*, vol. 60, 2009.

[11] R. Teasell, N.A.Bayona, and J. Bitensky, "Plasticity and reorganization of the brain poststroke," *Topics in Stroke Rehabilitation*, vol. 12, no. 3, pp. 11–26, 2005.

[12] E. Guglielmelli, M. Johnson, and T. Shibata, "Guest editorial special issue on rehabilitation robotics," *IEEE Transactions on Robotics*, vol. 25, 2009.

[13] B. Massa, S. Roccella, M. C. Carrozza, and P. Dario, "Design and development of an underactuated prosthetic hand," *Proceedings of the IEEE International Conference on Robotics and Automation*, vol. 4, 2002.

[14] D. Gunji, Y. Mizoguchi, S. Teshigawara, M. Aiguo, A. Namiki, M. Ishikawaand, and M. Shimojo, "Grasping force control of multi-fingered robot hand based on slip detection using tactile sensor," *IEEE International Conference on Robotics and Automation*, 2008.

[15] L. Zollo, S. Roccella, E. Guglielmelli, M. C. Carrozza, and P. Dario, "Biomechatronic design and control of an anthropomorphic artificial hand for prosthetic and robotic applications," *IEEE/ASME Transactions on Mechatronics*, vol. 12, no. 4, pp. 418–429, 2007.

[16] M. Carrozza, G. Cappiello, S. Micera, B. B. Edin, L. Beccai, and C. Cipriani, "Design of a cybernetic hand for perception and action," *Biological Cybernetics*, vol. 95, no. 6, pp. 629–644, 2006.

[17] C. L. Taylor and R. J. Schwarz, "The anatomy and mechanics of the human hand," *Artificial Limbs*, vol. 2, no. 2, pp. 22–35, 1955.

[18] O. van Nierop, A. van der Helm, K. J. Overbeeke, and T. J. P. Djajadiningrat, "A natural human hand model," *Visual Computer*, vol. 24, 2008.

[19] K. Kuczynski, "Carpometacarpal joint of the human thumb," *Journal of Anatomy*, vol. 118, no. 1, pp. 119–126, 1974.

[20] R. Yoshida, H. O. House, R. M. Patterson, M. A. Shah, and S. F. Viegas, "Motion and morphology of the thumb metacarpophalangeal joint," *Journal of Hand Surgery*, vol. 28, no. 5, pp. 753–757, 2003.

[21] A. Hollister, W. L. Buford, L. M. Myers, D. J. Giurintano, and A. Novick, "The axes of rotation of the thumb carpometacarpal joint," *Journal of Orthopaedich Research*, vol. 10, no. 3, pp. 454–460, 1992.

[22] Z. Li and J. Tang, "Coordination of thumb joints during opposition," *Journal of Biomechanics*, vol. 40, 2007.

[23] M. C. Hume, H. Gellman, h. McKellop, and R. H. Brumfield, "Functional range of motion of the joints of the hand," *Journal of Hand Surgery*, vol. 15, no. 2, pp. 240–243, 1990.

[24] P. Braido and X. Zhang, "Quantitative analysis of finger motion coordination in hand manipulative and gestic acts," *Human Movement Science*, vol. 22, 2004.

[25] J. Lin, Y. Wu, and T. Huang, "Modeling the constraints of the human hand motion," *Proceedings of the 5th Annual Federated Laboratory Symposium*, 2001.

[26] G. D. Kessler, L. F. Hodges, and N. Walker, "Evaluation of the cyberglove as a whole hand input device," *ACM Transactions on Computer-Human Interaction*, vol. 2, 1995.

[27] "Vicon system webpage," *http://www.vicon.com*.

[28] "Kinect motion sensing device webpage," *http://mirror2image.wordpress.com /2010/11/30/how-kinect-works-stereo-triangulation*.

[29] M. Santello and J. Soechting, "Gradual molding of the hand to object contours," *Journal of Neurophysiology*, vol. 79, no. 3, pp. 1307–1320, 1998.

[30] C. L. Mackenzie and T. Iberall, *The Grasping Hand*. Elsevier-North Holland, 1994.

[31] M. Jeannerod, M. Arbib, G. Rizzolatti, and H. Sakata, "Grasping objects: the cortical mechanisms of visuomotor transformation," *Trends in Neurosciences*, vol. 18, 1995.

[32] T. Feix, R. Pawlik, H. Schmiedmayer, J. Romero, and D. Kragic, "A comprehensive grasp taxonomy," *Robotics, Science and Systems Conference: Workshop on Understanding the Human Hand for Advancing Robotic Manipulation*, 2009.

[33] N. Kamakura, M. Matsuo, H. Ishii, F. Mitsuoboshi, and Y. Miura, "Patterns of static prehension in normal hands," *American Journal of Occupational Therapy*, vol. 4, no. 7, pp. 437–445, 1980.

[34] J. R. Napier, "The prehensile movements of the human hand," *Journal of Bone & Joint Surgery*, vol. 38-B, no. 4, pp. 902–913, 1956.

[35] L. Jones and S. Lederman, *Human Hand Function*. Oxford University Press, 2006.

[36] C. Taylor and R. Schwarz, "The anatomy and mechanics of the human hand," *Artificial Limbs*, vol. 2, no. 2, pp. 22–35, 1955.

[37] T. Iberall, *A neural model of human prehension*. PhD thesis, University of Massachussets, 1987.

[38] C. Ansuini, M. Santello, S. Massaccesi, and U. Castiello, "Effects of end-goal on hand shaping," *Journal of Neurophysiology*, vol. 95, 2006.

[39] I. M. Bullock and A. Dollar, "Classifying human manipulation behavior," *IEEE International Conference on Rehabilitation Robotics*, 2011.

[40] D. M. Lyons, "A simple set of grasps for a dextrous hand," *IEEE International Conference on Robotics and Automation*, 1985.

[41] B. Buchholz and T. Armstrong, "A kinematic model of the human hand to evaluate its prehensile capabilities," *Journal of Biomechanics*, vol. 25, no. 2, pp. 149–162, 1992.

[42] J. Park and J. Cheong, "Analysis of collective behavior and grasp motion in human hand," *International Conference on Control, Automation and Systems*, 2010.

[43] D. Guirintano, A. Hollister, W. Buford, D. Thompson, and L. Myers, "A virtual five-link model of the thumb," *Medical Engineering and Physics*, vol. 17, 1995.

[44] L. Y. Chang and Y. Matsuoka, "A kinematic thumb model for the act hand," *Proceedings of the IEEE International Conference on Robotics and Automation*, 2006.

[45] V. J. Santos and F. J. Valero-Cuevas, "Reported anatomical variability naturally leads to multimodal distributions of denavit-hartenberg parameters for the human thumb," *IEEE Transactions on Biomedical Engineering*, vol. 53, no. 2, pp. 155–163, 2006.

[46] M. Grebenstein, M. Chalon, G. Herzinger, and R. Siegwart, "A method for hand kinematics designers," *1st International Conference on Applied Bionics and Biomechanics*, 2010.

[47] P. Cerveri, E. D. Momi, N. Lopomo, G. Baud-Bovy, R. M. L. Barros, and G. Ferrigno, "Finger kinematic modeling and real-time hand motion estimation," *Annals of Biomedical Engineering*, vol. 35, no. 11, pp. 1989–2002, 2007.

[48] S. W. Lee, H. Chen, J. D. Towels, and D. G. Kamper, "Effect of finger posture on the tendon force distribution within the finger extensor mechanism," *Journal of Biomedical Engineering*, vol. 130, no. 5, pp. 2–25, 2008.

[49] A. Ikeda, Y. Kurita, and T. Ogasawara, "A tendon skeletal finger model for evaluation of pinching effort," *IEEE/RSJ International Conference on Robots and Systems*, 2009.

[50] Z. Li and J. Tang, "Coordination of thumb joints during opposition," *Journal of Biomechanics*, vol. 40, no. 3, pp. 502–510, 2007.

[51] W. Cooney, M. Lucca, E. Chao, and R. Linscheid, "The kinesiology of the thumb trapeziometacarpal joint," *Journal of Bone & Joint Surgery*, vol. 63A, 1981.

[52] S. Jacobsen, J. Wood, D. Knutti, and K. Biggers, "The Utah-MIT dextrous hand: work in progress," *International Journal of Robotics Research*, vol. 3, no. 4, pp. 21–50, 1984.

[53] M. Ali, K. Kyriakopoulos, and H. Stephanou, "The kinematics of the anthrobot-2 dextrous hand," *Proceedings IEEE International Conference on Robotics and Automation*, vol. 3, 1993.

[54] C. Lovchik and M. Diftler, "The robonaut hand. A dextrous robot hand for space," *Proceedings IEEE International Conference on Robotics and Automation*, 1999.

[55] M. Butterfass, H. Grebenstein, H. Liu, and G. Hirzinger, "DLR-Hand II. next generation of a dextrous robot hand," *Proceedings IEEE International Conference on Robotics and Automation*, vol. 1, 2001.

[56] M. Chalon, M. Grebenstein, T. Winmbock, and G. Herzinger, "The thumb: Guidelines for a robotic design," *IEEE/RSJ International Conference on Intelligent Robots and Systems*, 2010.

[57] C. M. G. Borghesan, G. Palli, "Design of tendon-driven robotic fingers: Modeling and control issues," *IEEE International Conference on Robotics and Automation*, 2010.

[58] L. D. Smet, M. Urlus, A. Spriet, and G. Fabry, "Metacarpophalangeal and interphalangeal flexion of the thumb: influence of sex and age, relation to ligamentous injury," *Acta Orthopaedica Belgica*, vol. 59, 1993.

[59] G. Stillfried and P. van der Smagt, "Movement model of a human hand based on magnetic resonance imaging (MRI)," *1st International Conference on Applied Bionics and Biomechanics*, 2010.

[60] M. Jenkins, H. Bamberger, L. Black, and R. Nowinski, "Thumb joint flexion. What is normal?," *Journal of Hand Surgery*, vol. 23, 1998.

[61] P. Hahn, H. Krimmer, A. Hradetzky, and U. Lanz, "Quantitative analysis of the linkage between the interphalangeal joints of the index finger: An in vivo study," *Journal of hand surgery*, vol. 20, 1995.

[62] I. Carpinella, P. Mazzoleni, M. Rabuffetti, R. Thorsen, and M. Ferrarin, "Experimental protocol for the kinematic analysis of the hand: definition and repeatability," *Gait & Posture*, vol. 23, 2006.

[63] N. Miyata, M. Kouchi, T. Kurihara, and M. Mochimaru, "Modeling human hand link structure from optical motion capture data," *IEEE/RSJ Internation Conference on Intelligent Robots and Systems*, 2004.

[64] C. Metcalf, S. Notley, P. Chappell, J. Burridge, and V. Yule, "Validation and application of a computational model for wrist and hand movements using surface markers," *IEEE Transactions on Biomedical Engineering*, vol. 55, no. 3, 2008.

[65] X. Zhang, P. Braido, S. Lee, R. Hefner, and M. Redden, "A normative database of thumb circumduction in vivo: Center of rotation and range of motion," *Human Factors*, vol. 47, no. 3, pp. 550–561, 2005.

[66] F. Su, Y. Chou, C. Yang, G. Lin, and K. An, "Movement of finger joints induced by synergistic wrist motion," *Clinical Biomechanics*, vol. 20, 2005.

[67] K. Khoshelham, "Accuracy analysis of kinect depth data," *ISPRS workshop Laser Scanning*, 2011.

[68] J. Kofman, X. Wu, T. Luu, and S. Verma, "Tepeoperation of a robot manipulator using a vision-based human-robot interface," *IEEE Transactions on Industrial Electronics*, vol. 52, no. 5, pp. 1206–1219, 2005.

[69] V. Pavlovic, R.Sharma, and T. Huang, "Visual interpretation of hand gestures for human computer interaction: A review," *IEEE Transactions on Pattern Analysis Machine Intelligence*, vol. 19, 1997.

[70] F. Quck, "Unencumbered gesture interaction," *IEEE Multimedia*, vol. 3, no. 3, pp. 36–47, 1996.

[71] J. Kuck and T. Huang, "Vision-based hand modeling and tracking for virtual teleconferencing and telecollaboration," *Proceedings of IEEE Conference on Computer Vision*, 1995.

[72] Y. Wu and T. Huang, "Hand modeling, analyisis, and recognition for vision-based human computer interaction," *IEEE Signal Processing Magazine*, 2001.

[73] Y. Wu and T. Huang, "View-independent recognition of hand postures," *Proceedings of IEEE Conference on Computer Vision and Pattern Recognition*, vol. 2, 2000.

[74] S. Lu, D. Metaxas, D. Samaras, and J. Oliensis, "Using multiple cues for hand tracking and model refinement," *Proceedings of IEEE Conference on Computer Vision and Pattern Recognition*, vol. 2, 2003.

[75] Y. Wu and T. Huang, "Capturing articulated human motion: A divide-and-conquer approach," *Proceedings of IEEE Interantion Conference on Computer Vision*, 1999.

[76] J. Lee and T. Kunii, "Model-based analysis of hand posture," *IEEE Computer Graphic Applications*, vol. 15, no. 5, pp. 77–86, 1995.

[77] M. Bray, E. Koller-Meier, and L. V. Gool, "Smart particle filtering for 3d hand tracking," *Proceedings of IEEE International Conference on Automatic Face & Gesture Recognition*, 2004.

[78] M. Isard and A. Blake, "Condensation-conditional density propagation for visual tracking," *International Journal of Computer Vision*, vol. 29, no. 1, pp. 5–28, 1998.

[79] J. Y. Lin, Y. Wu, and T. S. Huang, "3d model-based hand tracking using stochastic direct search method," *Proc. IEEE Int. Conf. Automatic Face & Gesture Recognition*, 2004.

[80] W. Chang, C. Chen, and Y. Hung, "Appearance-guided particle filtering for articulated hand tracking," *Proceedings of IEEE Computer Society Conference on Computer Vision and Pattern Recognition*, vol. 1, 2005.

[81] E. Trucco and A. Verri, *Introductory Techniques for 3D Computer Vision.* Prentice Hall.

[82] R. Hartley and A. Zisserman, *Multiple View Geometry in Computer Vision*. Berlin-Heidelberg: Cambridge University Press, 2000.

[83] S. Sarkka, A. Vehtari, and J. Lampinen, "Rao-blackwellized particle filter for multiple target tracking," *Proceedings of the 7th International Conference on Information Fusion*, vol. 8, no. 1, pp. 2–15, 2007.

[84] S. Sarkka, A. Vehtari, and J. Lampinen, "Rao-blackwellized Monte Carlo data association for multiple target tracking," *Proceedings of the International Conference on Information Fusion*, vol. 7, 2004.

[85] R. Chen and J. Liu, "Mixture Kalman filter," *Journal of the Royal Statistical Society: Series B*, vol. 62, no. 3, pp. 493–508, 2000.

[86] M. Santello, M. Flanders, and J. Soechting, "Postural hand synergies for tool use," *Journal of Neuroscience*, vol. 18, no. 23, pp. 105–115, 1998.

[87] C. Mason, J. Gomez, and T. Ebner, "Hand synergies during reach-to-grasp," *Journal of Neurophysiology*, vol. 86, no. 6, pp. 2896–2910, 2001.

[88] M. Roa and R. Suarez, "Regrasp planning in the grasp space using independent regions," *IEEE/RSJ International Conference on Intelligent Robots and Systems*, 2009.

[89] W. Lee and X. Zhang, "Development and evaluation of an optimization-based model for power-grip posture prediction," *Journal of Biomechanics*, vol. 38, 2005.

[90] L. Zollo, S. Roccella, R. Tucci, B. Siciliano, E. Guglielmelli, M. Carrozza, and P. Dario, "Biomechatronic design and control of an anthropomorphic artificial hand for prosthetics and robotic applications," *IEEE/ASME Transactions on Mechatronics*, vol. 12, no. 4, pp. 418–429, 2007.

[91] T. Flash and N. Hogan, "The coordination of arm movements: an experimentally confirmed mathematical model," *Journal of Neurophysiology*, vol. 5, 1985.

[92] J. Friedman and T. Flash, "Trajectory of the index finger during grasping," *Experimental Brain Research*, vol. 196, 2009.

[93] D. Kamper, E. Cruz, and M. Siegel, "Stereotypical fingertip trajectories during grasp," *Journal of Neurophysiology*, vol. 90, no. 6, pp. 3702–3710, 2003.

[94] F. Cordella, L. Zollo, A. Salerno, E. Guglielmelli, and B. Siciliano, "Experimental validation of a reach-and grasp optimization algorithm inspired to human arm-hand control," *International Conference of the IEEE Engineering in Medicine and Biology Society*, 2011.

[95] J. Lukos, C. Ansuini, and M. Santello, "Choice of contact points during multidigit grasping: effect of predictability of object center of mass location," *Journal of Neuroscience*, vol. 27, no. 14, pp. 3894–3903, 2007.